Biogeosciences, 5, 385–406, 2008
www.biogeosciences.net/5/385/2008/


Biogeosciences

# The impact on atmospheric $CO_2$ of iron fertilization induced changes in the ocean's biological pump

**X. Jin[1], N. Gruber[2,3], H. Frenzel[1], S. C. Doney[4], and J. C. McWilliams[3]**

[1]Institute of Geophysics and Planetary Physics (IGPP), UCLA, Los Angeles, CA 90095, USA
[2]Environmental Physics, Institute of Biogeochemistry and Pollutant Dynamics, ETH Zürich, Zürich, Switzerland
[3]IGPP & Department of Atmospheric and Oceanic Sciences, UCLA, Los Angeles, CA 90095, USA
[4]Dept. of Marine Chemistry and Geochemistry, Woods Hole Oceanographic Institution, Woods Hole, MA 02543-1543, USA

Received: 12 October 2007 – Published in Biogeosciences Discuss.: 19 October 2007
Revised: 25 January 2008 – Accepted: 13 February 2008 – Published: 18 March 2008

**Abstract.** Using numerical simulations, we quantify the impact of changes in the ocean's biological pump on the air-sea balance of $CO_2$ by fertilizing a small surface patch in the high-nutrient, low-chlorophyll region of the eastern tropical Pacific with iron. Decade-long fertilization experiments are conducted in a basin-scale, eddy-permitting coupled physical/biogeochemical/ecological model. In contrast to previous studies, we find that most of the dissolved inorganic carbon (DIC) removed from the euphotic zone by the enhanced biological export is replaced by uptake of $CO_2$ from the atmosphere. Atmospheric uptake efficiencies, the ratio of the perturbation in air-sea $CO_2$ flux to the perturbation in export flux across 100 m, integrated over 10 years, are 0.75 to 0.93 in our patch size-scale experiments. The atmospheric uptake efficiency is insensitive to the duration of the experiment. The primary factor controlling the atmospheric uptake efficiency is the vertical distribution of the enhanced biological production and export. Iron fertilization at the surface tends to induce production anomalies primarily near the surface, leading to high efficiencies. In contrast, mechanisms that induce deep production anomalies (e.g. altered light availability) tend to have a low uptake efficiency, since most of the removed DIC is replaced by lateral and vertical transport and mixing. Despite high atmospheric uptake efficiencies, patch-scale iron fertilization of the ocean's biological pump tends to remove little $CO_2$ from the atmosphere over the decadal timescale considered here.

*Correspondence to:* X. Jin
(xjin@ucla.edu)

## 1 Introduction

The ocean's biological pump is a key regulator of atmospheric $CO_2$. Changes of the biological pump appear to have contributed substantially to the glacial-interglacial changes in atmospheric $CO_2$ (Sarmiento and Toggweiler, 1984; Martin, 1990; Kohfeld et al., 2005; Sigman and Haug, 2003), and likely will have a substantial impact on future atmospheric $CO_2$ levels (Sarmiento et al., 1998; Joos et al., 1999). While the sign of the response of atmospheric $CO_2$ to changes in the biological pump is well established, the magnitude of the change in atmospheric $CO_2$ for a given change in the biological pump is neither well known nor well understood.

When one thinks about the impact of the ocean's biological pump on the air-sea balance of $CO_2$, one often tends to consider only the downward (export) flux of biogenic carbon (organic carbon and mineral $CaCO_3$). However, the air-sea $CO_2$ balance induced by the biological pump is as strongly determined by the upward (circulation and mixing-driven) transport of the dissolved inorganic carbon (DIC) that stems from the remineralization/dissolution of the exported biogenic carbon. In steady state, the upward and downward components of the biological pump balance each other globally (disregarding the relatively small flux of organic carbon that is added to the ocean from rivers and is buried in sediments), so that the biological pump has a global net air-sea $CO_2$ flux of zero. But this does not have to be the case locally. In fact, the local balance between the upward supply of biologically derived DIC and the export flux of biogenic carbon determines the magnitude and direction of the air-sea $CO_2$ fluxes induced by the biological pump (Murnane et al., 1999; Gruber and Sarmiento, 2002). Surface regions, to which more biologically derived DIC is transported than

biogenic carbon is removed from, tend to lose $CO_2$ to the atmosphere. In such cases, we term the biological pump as inefficient (Sarmiento and Gruber, 2006). In contrast, surface regions, from which more biogenic carbon is removed than biologically derived DIC is added to, tend to gain $CO_2$ from the atmosphere. In such cases, the biological pump is efficient. Therefore, the primary means for the biological pump to change atmospheric $CO_2$ is by altering its efficiency.

Fertilization with iron is potentially a powerful option to increase the efficiency of the biological pump and to draw $CO_2$ from the atmosphere. An advantage of this method to perturb the ocean's biological pump is that it affects initially only the downward (export) component. It differs from climate change (Sarmiento et al., 1998; Joos et al., 1999; Plattner et al., 2001), in which often both components of the biological pump are initially altered, making it difficult to isolate the mechanisms that determine the changed air-sea balance of $CO_2$. Iron fertilization works because there exist extensive high-nutrient/low-chlorophyll (HNLC) regions of the ocean, such as the Southern Ocean and the eastern tropical Pacific, where biological productivity is limited by iron (Martin et al., 1990). Although this iron limitation hypothesis has been confirmed by a series of iron fertilization experiments (Martin et al., 1994; Boyd et al., 2000, 2004; Coale et al., 2004; de Baar et al., 2005; Boyd et al., 2007), the direct experimental demonstration that iron fertilization induces an increased downward transport of biogenic carbon has remained elusive (e.g., Buesseler and Boyd, 2003). Nevertheless, evidence from the geological past (e.g., Sigman and Haug, 2003) and from natural (long-term) iron fertilization experiments (e.g., Blain et al., 2007) strongly suggest that this is indeed the case. Therefore, it is not surprising that the use of iron fertilization as a means to slow down the anthropogenically driven buildup of atmospheric $CO_2$ has intrigued scientists, venture capitalists, and the public alike (Martin, 1990; Chisholm et al., 2001; Buesseler et al., 2008). However, most research to date has shown that the maximum realizable carbon sink is relatively small (Peng and Broecker, 1991; Joos et al., 1991; Sarmiento and Orr, 1991; Orr and Sarmiento, 1992; Aumont and Bopp, 2006) and the unintended consequences potentially large (Chisholm et al., 2001; Jin and Gruber, 2003; Schiermeier, 2003).

A measure of the overall impact of the addition of iron on atmospheric $CO_2$ is the carbon-to-iron fertilization ratio, which reflects how much additional $CO_2$ is taken up from the atmosphere for a given amount of iron added to the ocean (see Appendix A for details). This fertilization ratio can be split into an efficiency part that reflects how much $CO_2$ is taken up from the atmosphere per unit change in biological export (termed the atmospheric uptake efficiency, $e_{\text{uptake}}$), and into a biological iron utilization ratio that reflects how a given amount of added iron stimulates the biological export of carbon (termed the iron utilization ratio, $R^{\text{C:Fe}}_{\text{iron util}}$) (Sarmiento et al., 2008[1]). By definition, the product of the atmospheric uptake efficiency and the biological iron utilization ratio is the fertilization ratio.

The atmospheric $CO_2$ uptake efficiency describes how the inorganic carbon is replaced that has been fixed into biogenic carbon in response to the fertilization and then exported to depth. If all of this carbon comes from the atmosphere, the atmospheric uptake efficiency is unity. However, in most cases, the atmospheric uptake efficiency is smaller than one. This is because of a number of mechanisms: (i) Lateral mixing and transport, (ii) $CaCO_3$ formation, (iii) buffering by the carbonate system, and (iv) a global-scale efflux of $CO_2$ from the ocean in response to the lowered atmospheric $CO_2$ concentration. Most large-scale iron fertilization modeling studies conducted so far on the basis of simple nutrient restoring models, i.e. models that do not include the iron cycle per se, but mimic iron fertilization by assuming that all macronutrients are used up in the euphotic zone, found atmospheric uptake efficiencies between about 10% and 40% (Peng and Broecker, 1991; Joos et al., 1991; Sarmiento and Orr, 1991; Jin and Gruber, 2003). Similarly low atmospheric uptake efficiencies were found recently by Gnanadesikan et al. (2003), who studied the impact of short-time and patch-scale iron fertilization on the air-sea balance of $CO_2$ also using a nutrient restoring model. By contrast, the atmospheric uptake efficiencies that we report on in this study based on fertilizing patch-size regions in the eastern tropical Pacific are much larger, i.e. as high as 93%. Our study as well the recent ones by Aumont and Bopp (2006) and Moore et al. (2006), which also simulated such high atmospheric uptake efficiencies, differ fundamentally from the previous nutrient restoring model simulations in that the iron cycle was considered explicitly in the models and therefore iron fertilization experiments were undertaken by actually adding iron to the ocean.

The goal of this paper is to determine the factors that control the atmospheric uptake efficiency, and to explain why we find so much larger atmospheric uptake efficiencies than previous studies. Although this study uses iron fertilization as a means to change the biological export of carbon, the answers we provide are relevant for any change in the ocean's biological pump, irrespective of the factors that cause this change. This is because the atmospheric uptake efficiency is essentially a metric of how important the biological pump is in controlling atmospheric $CO_2$. This study thus follows a trend in that the motivation to undertake iron fertilization studies is increasingly determined by the unique opportunities that such manipulations offer to understand the responses of marine ecology and biogeochemistry to perturbations (see e.g. Boyd et al., 2005 and Boyd et al., 2007).

The most important finding of this study is that the primary factor controlling the atmospheric uptake efficiency is

[1]Sarmiento, J. L., Slater, R., Maltrud, M. E., and Dunne, J.: Model sensitivity studies of patchy iron fertilization to sequester $CO_2$, Biogeosciences, in preparation, 2008.

where within the euphotic zone the stimulation of production and export occurs. The closer to the air-sea surface DIC is transformed to biogenic carbon and exported, the higher the likelihood that this carbon is replaced from the atmosphere, resulting in high uptake efficiencies. If the stimulus occurs near the bottom of the euphotic zone, the atmospheric uptake efficiency is low, as most of the removed DIC will tend to come from the surrounding water. Fertilization with iron from above tends to stimulate most additional carbon production and export near the surface, explaining our high efficiencies. By contrast, nearly all previous studies employed a nutrient restoring approach to emulate iron fertilization, thereby tending to stimulate enhanced biological export near the bottom of the euphotic zone, thus explaining their low atmospheric uptake efficiencies.

The paper is organized as follows. We first introduce the coupled physical/biogeochemical/ecological model and then describe the various numerical experiments. Since this model setup is new, we next evaluate a number of key model results with observations, focusing on the biogeochemical aspects. This is followed by the core part of the paper, which are the results and their discussion. We close the paper with a brief summary and our conclusions.

## 2 Methods

### 2.1 Model description

We investigate the impact of iron fertilization on biological export production and atmospheric $CO_2$ using a coupled physical/biogeochemical/ecological model of the Pacific Ocean at eddy-permitting horizontal resolution. The physical model we use is the Regional Oceanic Modeling System (ROMS) (Haidvogel et al., 2000; Shchepetkin and McWilliams, 2005), configured for a whole Pacific domain (north of 45° S) at a horizontal resolution of about 0.5° (about 50 km). This resolution permits the formation of eddies and other mesoscale phenomena (e.g. tropical instability waves), but does not fully resolve them. As a result, the model simulated eddy kinetic energy is substantially smaller than observed. In the vertical, ROMS uses a sigma-coordinate system that is terrain following with a total of 30 vertical layers. In the open ocean of the eastern equatorial Pacific Ocean, 11 layers are within the uppermost 100 m, i.e. about the depth of the euphotic zone. This Pacific configuration of ROMS has closed lateral boundaries, making our results near the southern boundary at 45° S unrealistic. We therefore evaluate the model's performance only for the region north of 35° S. At the surface, the model is forced with a monthly climatology of heat and freshwater fluxes and wind stress based on the NCEP reanalysis (Kalnay et al., 1996). Explicit temperature restoring terms are used to keep the model's sea-surface temperature from drifting excessively. The physical model was spun up from rest for 10 years, using initial conditions for temperature and salinity from the World Ocean Atlas 2001 (Conkright et al., 2002).

The biogeochemical/ecological model is the Biogeochemical Elemental Cycling model of Moore et al. (2004) (BEC). Here, we only give a short summary of the model except for the iron cycle that we describe in more depth. The ecological model considers four phytoplankton functional groups, picoplankton, diatoms, coccolithophores, diazotrophs (Trichodesmium spp.), which compete for the available nutrients and light and are grazed upon by an adaptive zooplankton class. Growth of the different phytoplankton functional groups are limited by the available nitrogen (nitrate, ammonium), phosphorus (phosphate), silicon (silicic acid), and iron (bio-available ferric and ferrous iron), which they need in different proportions. The diazotrophs get all required nitrogen from $N_2$ gas with growth limited at temperatures below 15°C. The coccolithophorids are not explicitly modeled, but their growth and the resulting calcification is parameterized as a variable fraction of picoplankton production. Diatoms are the only functional group requiring silicon. Additional state variables include dissolved organic matter and sinking detritus, whereby the ballast model of Armstrong et al. (2002) is used. As is the case in the global implementation of this model by Moore et al. (2004), this version has fixed stoichiometric C:N:P ratios for each functional group, while the Fe ratios vary depending on growth rate. The parameters of the model are also from Moore et al. (2004). This model configuration does not include a parameterization for denitrification, so that possible impacts of iron fertilization on this process are not considered in our simulations. Nor does our model include the cycling of $N_2O$, for which we have shown substantial alterations in response to successful iron fertilizations (Jin and Gruber, 2003). The initial conditions for dissolved oxygen, phosphate, nitrate, and silicate are taken from the World Ocean Atlas 2001 (Conkright et al., 2002), while those for dissolved inorganic carbon and alkalinity are from GLODAP (Key et al., 2004). All other variables of the biogeochemical/ecological model are initialized using the results from the global model of Moore et al. (2004). The coupled physical/biogeochemical/ecological model was run for 10 years before any experiments were conducted. Atmospheric $pCO_2$ is fixed at 278 ppmv. As a result, our computed atmospheric uptake efficiencies do not include a global efflux effect that arises in response to the lowered atmospheric $CO_2$. As discussed later, our neglecting of this effect causes our computed atmospheric uptake efficiencies to be upper-bound estimates.

The iron cycle in the model of Moore et al. (2004) is of reduced complexity, similar to those recently incorporated into large-scale biogeochemical models by other groups (e.g., Aumont et al., 2003; Dutkiewicz et al., 2005; Gregg et al., 2003). The forms of iron considered are dissolved iron, which is assumed to be bioavailable, iron associated with organic matter in the various organic matter pools, iron

associated with dust particles, and scavenged iron. Of those, only dissolved iron and the organically bound iron are explicitly modeled as state variables.

For dissolved iron, three processes are considered: External sources, biological uptake and remineralization, and scavenging by sinking particles. The external sources include atmospheric dust and shallow sediments. The deposition flux of iron from atmospheric dust is based on the dust climatology of Luo et al. (2003) and the assumption that the dust has a fixed iron content of 3.5% by weight. The surface solubility of the iron is 2% and it is assumed that all the dissolved iron is bioavailable. Additional 3% of the iron deposited by the dust is dissolved as the dust particles settle through the water column, with a dissolution length scale of 600 m. The remaining dust is treated as ballast, with a dissolution length scale of 40 000 m. All sediment regions down to a depth of 1100 m are assumed to be a source of sedimentary iron, with a constant source strength of 0.73 mmol Fe $m^{-2}$ $yr^{-1}$.

Biological uptake of dissolved iron is stoichiometrically linked with the biological fixation of carbon using, in the case of phytoplankton, iron concentration dependent Fe-to-C uptake ratios. For zooplankton, a constant Fe-to-C ratio is assumed. The organically bound iron is remineralized back to dissolved iron according to the Fe-to-C ratio of the remineralizing organic matter, i.e. without fractionation.

The model's dissolved iron is scavenged by sinking particles, including dust and particulate organic matter (POM). In order to mimic the effect of ligands, the scavenging rate is drastically reduced at low ambient dissolved iron concentrations ($<$0.5 nM). The scavenging is enhanced at elevated iron concentrations ($>$ 0.6 nM). Sinking POM is assumed to be responsible for 10% of the total scavenging. This scavenged iron is released back to the water column when the POM is remineralized. The remaining 90% of the scavenged iron is lost to sediments and hence permanently removed from the water column.

### 2.2 Iron fertilization experiments

The aim of our iron fertilization experiments is to determine the factors that control the atmospheric uptake efficiency. In particular, we consider the role of the size of the fertilized region, the duration of the fertilization, and the vertical structure of the stimulated export production.

Our standard experiment consists of the fertilization of a medium size patch ($3.7\times10^5$ $km^2$) in the eastern tropical Pacific Ocean, close to where the IronEx II experiment was conducted (Coale et al., 1996b), i.e. 104° W, 3.5° S. For the fertilization, iron is continuously added into the surface layer of the model at a constant rate of 0.02 mmol Fe $m^{-2}$ $yr^{-1}$ over ten years. All added iron is assumed to be bioavailable, but is subject to mixing, transport, scavenging, and biological uptake and remineralization. All changes, e.g. changes in biological production, export production, air-sea fluxes of $CO_2$, are then determined relative to a control simulation that is run for the same duration from the same initial state, except that no additional iron is added.

The impact of the size of the fertilized region on the atmospheric uptake efficiency is determined using a suite of 4 additional experiments, ranging in size from $3.7\times10^3$ $km^2$ (about 60×60 km) (TINY) to the entire Pacific ($15\times10^7$ $km^2$) (X-LARGE) (cf. Table 1). The impact of the duration of the fertilization is studied with two sensitivity experiments. In the 3MON-repeat case, we fertilize the standard patch for three months every year, while in the 3MON-onetime case, the ocean is fertilized for three months in the first year only (Table 1). All sensitivity experiments use the same perturbation iron fluxes per square meter as the standard experiment.

In order to investigate the role of the depth distribution of the stimulated export production on the atmospheric uptake efficiency, we designed a series of additional experiments. In the first two simulations, we increased the penetration of light into the upper ocean by reducing the attenuation coefficient for chlorophyll and water by half and by a factor of four, respectively (LIGHT-DEPTH experiments, see Table 1). In the second two (more extreme) experiments, we entirely removed the light limitation for phytoplankton growth down to either 75 m or 50 m, respectively (LIGHT-UNLIM experiments, Table 1). These changes led to a substantial enhancement of phytoplankton growth at the lower levels of the euphotic zone. In order to avoid an excessive growth of coccolithophorids, which would alter the results through their differential impact on the air-sea $CO_2$ balance, we limited their growth in the fertilized area by fixing the ratio of $CaCO_3$ production to picoplankton production, so that their contribution to organic matter export remains roughly unchanged.

In a final set of simulations, we evaluated the impact of the amount of iron added. In the first experiment, we doubled the iron input that is supplied to the surface ocean in the control simulation. In the second experiment, we removed the iron limitation of the phytoplankton growth. Rather than adding so much iron to the ocean that it becomes unlimiting, we achieved the same effect simply by manipulating the growth terms for the phytoplankton. For these latter two experiments, we perturbed the entire domain of our model.

In all simulations, the atmospheric $pCO_2$ is kept constant at 278 ppmv. Therefore, our results do not include the global-scale efflux of $CO_2$ from the ocean, which is induced by the lowered atmospheric $pCO_2$ (Gnanadesikan et al., 2003). Since this efflux will reduce the atmospheric uptake efficiency, our results will be higher than those based on simulations with an interactive atmospheric $CO_2$ reservoir. Sarmiento et al. (2008)[1] show that over 10 years, this effect results in a roughly 20% reduction of the atmospheric uptake efficiency, largely independent of the details of the experiment. Over 100 years, the effect causes about a 50% reduction.

**Table 1.** Summary of iron fertilization experiments performed with ROMS-BEC. All simulations are run for 10 years.

| Experiment | Location[a] | Area ($10^3$km$^2$) | Iron Flux (mmol m$^{-2}$yr$^{-1}$) | Comments |
|---|---|---|---|---|
| STANDARD | ETSP (101.6° W–106° W; 6.1° S–0.6° S) | 370 | 0.02 | Standard experiment |
| TINY | ETSP (104° W; 3.5° S ) | 3.7 | 0.02 | one model grid cell |
| SMALL | ETSP (103.1° W–105° W; 4.8° S–2.4° S) | 92 | 0.02 | |
| LARGE | ETP (87.7° W–137.2° W; 14.4° S–3.7° N) | 11 000 | 0.02 | entire ETP |
| X-LARGE | Pacific | 150 000 | 0.02 | entire Pacific |
| 3MON-onetime | ETSP (101.6° W–106° W; 6.1° S–0.6° S) | 370 | 0.02 | 3 months only in first year |
| 3MON-repeat | ETSP (101.6° W–106° W; 6.1° S–0.6° S) | 370 | 0.02 | 3 months every year (Aug–Oct) |
| LIGHT-DEPTH-2 | ETSP (101.6° W–106° W; 6.1° S–0.6° S) | 370 | 0 | reduce attenuation coefficient by half above 75 m |
| LIGHT-DEPTH-4 | ETSP (101.6° W–106° W; 6.1° S–0.6° S) | 370 | 0 | reduce attenuation coefficient by one fourth above 75 m |
| LIGHT-UNLIM-75 m | ETSP (101.6° W–106° W; 6.1° S–0.6° S) | 370 | 0.02 | no light limitation to 75 m |
| LIGHT-UNLIM-50 m | ETSP (101.6° W–106° W; 6.1° S–0.6° S) | 370 | 0.02 | no light limitation to 50 m |
| PAC-2×Fe | Pacific | 150 000 | 2× | double iron input |
| PAC-iron-unlim | Pacific | 150 000 | – | no iron limitation |

[a] All patches are centered at 104° W, 3.5° S. ETSP: Eastern Tropical South Pacific; ETP: Eastern Tropical Pacific.

## 3 Model evaluation

Before proceeding to the results, it is necessary to establish the credentials of our newly coupled model (ROMS-BEC). Given our aim to assess the impact of iron fertilization induced changes in the biological pump on atmospheric $CO_2$, one ideally would like to evaluate the model vis-à-vis such experiments. However, the data available from the IronEx II experiment in the tropical Pacific are rather limited (Coale et al., 1996b). In particular, these data cover only the initial response of the upper ocean ecosystem to the iron addition, leaving out the most relevant aspect of the experiment in the context of our study here, i.e. the change in the export of biogenic carbon. Therefore, we are therefore restricted in our evaluation of the model to the analyses of the climatological mean state as observed remotely by satellites (chlorophyll) and measured in situ (nutrients and iron). Here, we present only a summary; more details are provided in Appendices B and C, especially with regard to a more quantitative assessment on the basis of Taylor diagrams (Taylor, 2001).

The model reproduces the observed annual-mean large-scale patterns of surface chlorophyll derived from SeaWiFS imagery reasonably well (Fig. 1a and c). In fact, compared to the global-scale results of Moore et al. (2004), our Pacific-only model at eddy-permitting resolution yields somewhat higher levels of agreement, particularly with regard to resolving aspects of the elevated productivity in the coastal upwelling regions along the western margin of the Americas. Perhaps the most important deficiency is found in the central equatorial Pacific, where the model simulates annual mean chlorophyll concentrations that are two to three times higher than those observed.

Similar strengths and deficiencies of the model are found for surface nitrate (Fig. 1b and d). The model is successful in simulating the broad characteristics of the annual mean surface nitrate distribution synthesized from shipboard measurements (Conkright et al., 2002), but there are a couple of notable differences. In most areas of the subarctic North Pacific, the model's surface nitrate concentrations are too low and model values are higher near the Bering Sea boundary, while in the eastern tropical Pacific away from the equator, the tongue of elevated nitrate extends much further southward than seen in the observations.

In summary, ROMS-BEC is rather successful in modeling the main biogeochemical characteristics of the Pacific, with low nutrient/low chlorophyll, i.e. oligotrophic, conditions characterizing the subtropical gyres, and with HNLC conditions prevailing in the eastern tropical Pacific and in part of the high latitudes of the North Pacific. The deficiencies in the model are most likely due to the interaction of biases in the model physics with errors in the ecosystem/biogeochemical model (see Appendix C for further discussions).

Although clearly present, it turns out that these model biases have only a limited impact on our main results. This is because our primary focus is on the atmospheric uptake efficiency, i.e. a ratio, which is not expected to be sensitive to spatial mismatches in the model vis-à-vis observations. In fact, the somewhat overly broad HNLC conditions in the eastern tropical Pacific make the iron fertilization experiments actually less sensitive to our choice of location and provide for the necessary background to undertake a wide range of experiments.

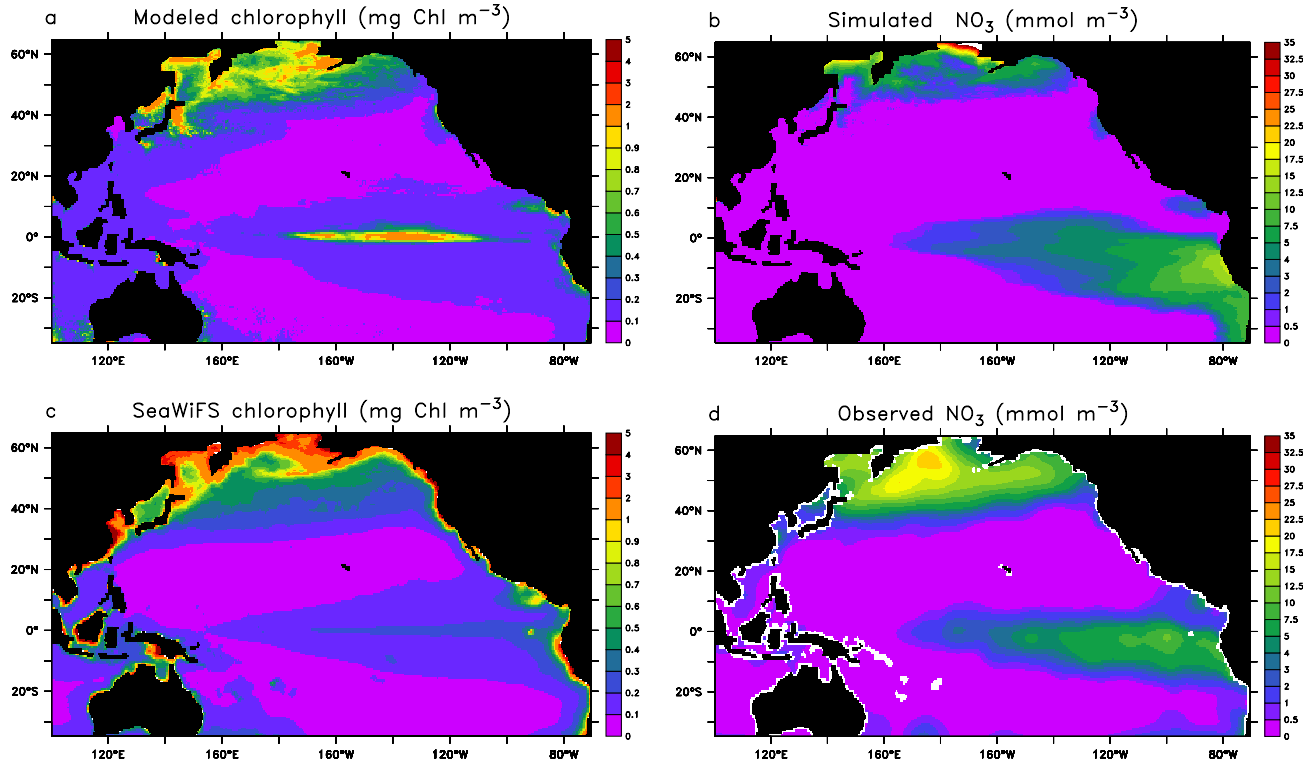


**Fig. 1.** Comparison of modeled and observed annual mean surface ocean properties. **(a)** Surface chlorophyll and **(b)** nitrate distribution as modeled by ROMS-BEC; **(c)** and **(d)**, as (a) and (b) but as observed. The chlorophyll data are from the SeaWiFS project and represent the mean for the years 1998 through 2004. They were obtained from the Distributed Active Archive Center (DAAC) at NASA Goddard in Greenbelt, MD (http://daac.gsfc.nasa.gov). The nitrate observations are from the World Ocean Atlas 2001 (Conkright et al., 2002).

## 4 Results

### 4.1 Effects of fertilization

In the standard case, the addition of iron for 10 years to the eastern tropical Pacific induces a strong and persistent phytoplankton bloom with chlorophyll levels reaching 2 mg Chl m$^{-3}$ (Fig. 2a, b), representing a roughly fivefold increase in surface chlorophyll. Inside the fertilized patch, depth integrated net primary production (NPP) is enhanced by up to 25 mol C m$^{-2}$ yr$^{-1}$, which corresponds to a roughly 30% increase relative to the unperturbed case (Fig. 3a, b). Surface nitrate becomes depleted (Fig. 2c, d), and the reduction of surface ocean DIC by more than 30 mmol m$^{-3}$ (Fig. 2e, f) leads to a drop in $pCO_2$ of more than 40 $\mu$atm (Fig. 2g, h). This reduction turns part of the fertilized area, which is normally a strong source of $CO_2$ to the atmosphere, into a sink (Fig. 3e, f). The magnitude of the changes in NPP, chlorophyll, DIC, nitrate, and $pCO_2$ are comparable to those observed during the most successful iron fertilization experiments (see e.g. de Baar et al. (2005) for a summary).

After 10 years, the impact of the iron addition extends far beyond the fertilized patch. This is particularly evident for surface nitrate (Fig. 2c, d), where the depletion induced near the fertilization site leads to reduced nitrate concentrations downstream extending for several thousand kilometers in southwesterly direction. But also the region of anomalous low $pCO_2$ and thus anomalous uptake of $CO_2$ from the atmosphere (Fig. 3e, f) extends over an area that is more than 5 times larger than the actually fertilized patch. One mechanism is simply the horizontal spreading of the added iron, leading to enhanced phytoplankton production well beyond the fertilization site. However, as evident from the chlorophyll changes (Fig. 2b), which extend only perhaps twofold outside the fertilized patch, this mechanism can explain only a part of the large extent of the region that is characterized by substantial $pCO_2$ reductions. The more important mechanism is the relatively slow kinetics of the exchange of $CO_2$ across the air-sea interface. Given an equilibration time scale for the exchange of $CO_2$ across the air-sea interface of several months (Sarmiento and Gruber, 2006) surface waters that contain anomalously low $pCO_2$ can be laterally spread for several additional months beyond the region of elevated production before the $CO_2$ deficiency is removed by uptake from the atmosphere.

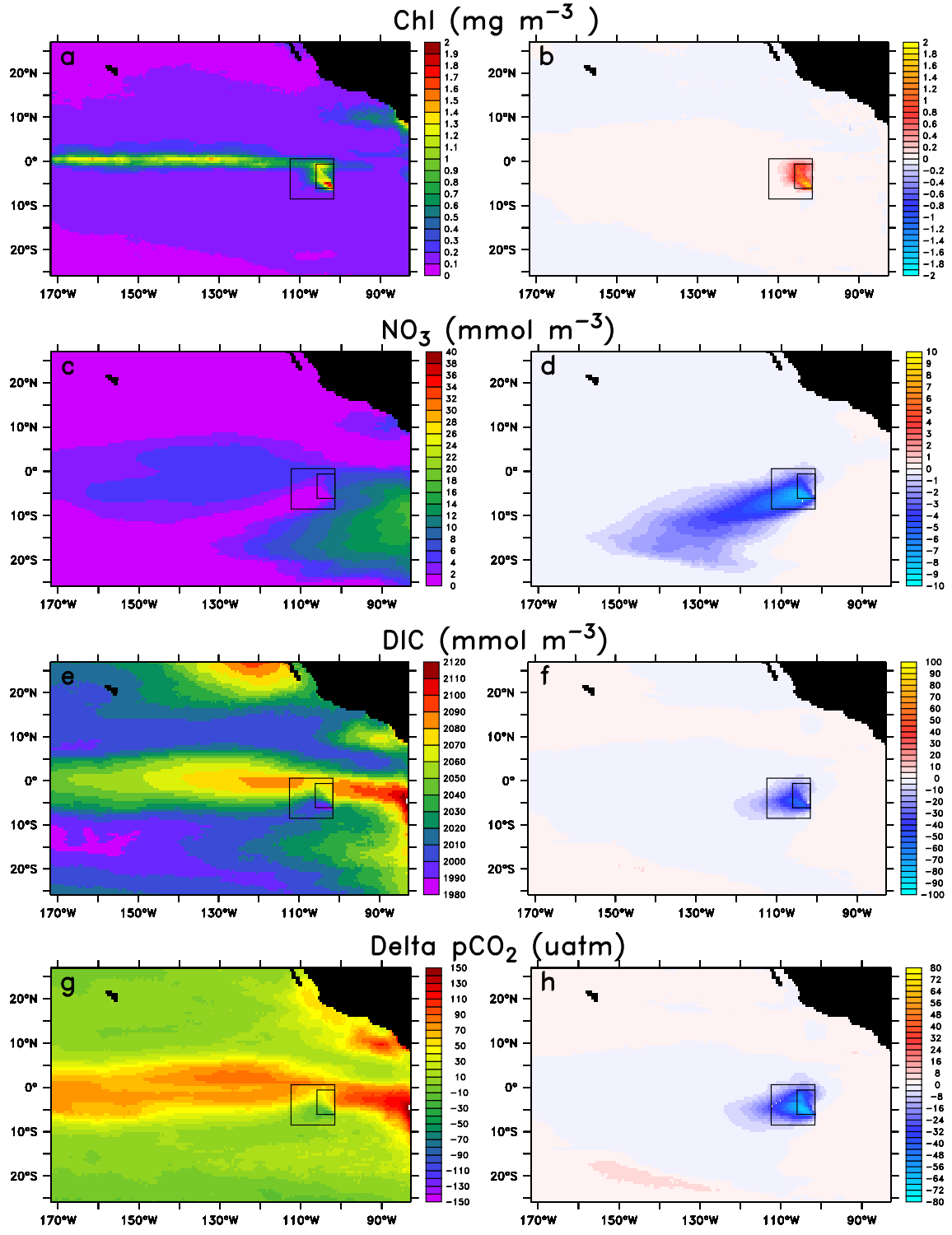


**Fig. 2.** Maps of the modeled response of surface ocean properties to the addition of iron for 10 years in the Eastern Tropical Pacific. The fertilized area is centered at 104° W, 3.5° S and its boundaries are marked by the inner box. The left column shows the model simulated fields after 10 years, while the right column depicts the changes relative to a control simulation (fertilization minus control). **(a)** and **(b)** chlorophyll (mg Chl $m^{-3}$); **(c)** and **(d)** nitrate (mmol $m^{-3}$); **(e)** and **(f)** dissolved inorganic carbon (mmol $m^{-3}$); **(g)** and **(h)** air-sea difference of the partial pressure of $CO_2$ ($\Delta pCO_2$) ($\mu$atm). Positive $\Delta pCO_2$ indicates surface ocean supersaturation. Results are shown for the STANDARD case, averaged for the 10th year of the simulation. The inner box is the region of our STANDARD case and the outer box is the region where we calculate our regional properties, e.g., in Table 2.

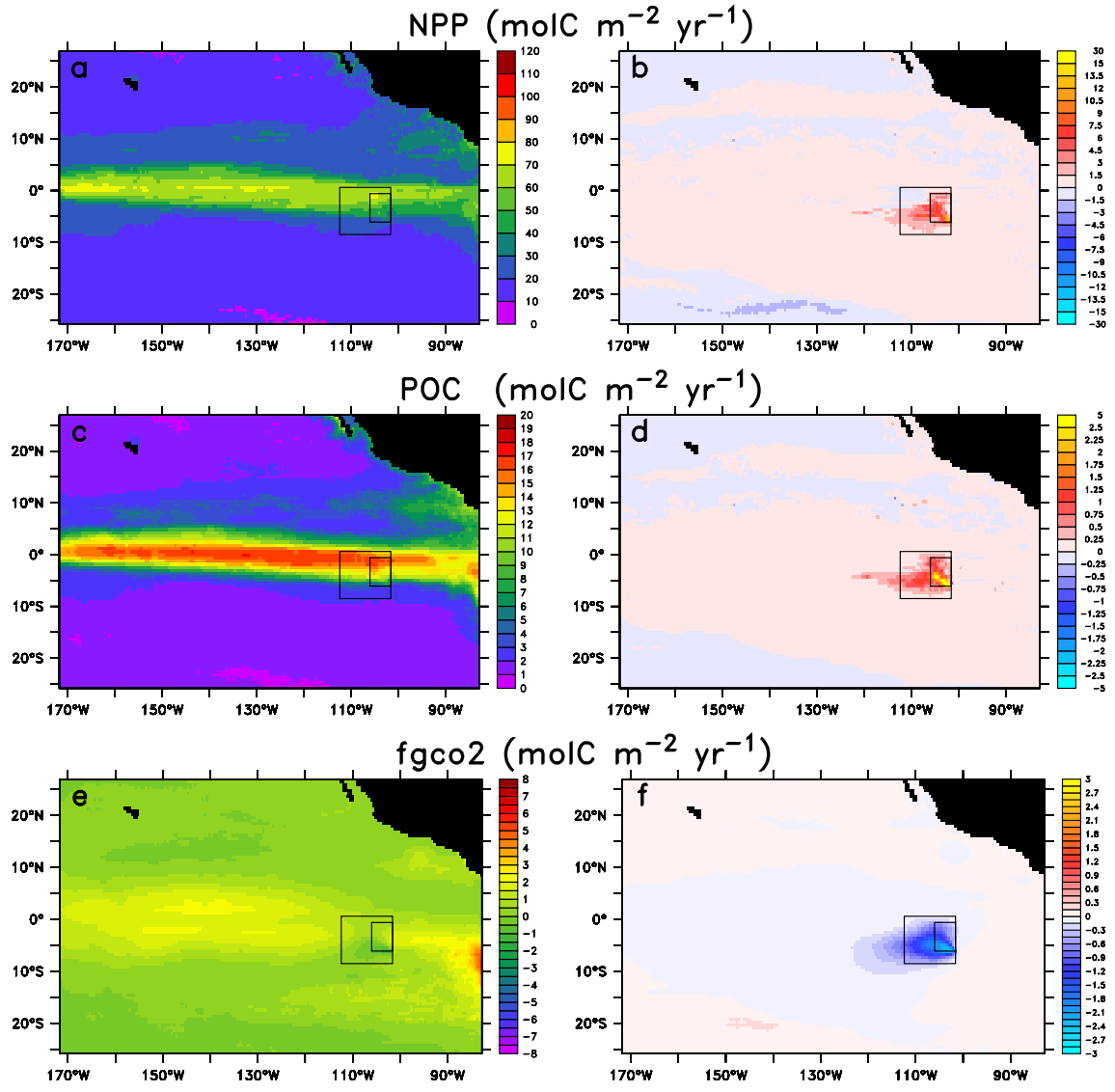


**Fig. 3.** As Fig. 2, except for **(a)** and **(b)** vertically integrated net primary production (0–100 m) (mol C m$^{-2}$ yr$^{-1}$); **(c)** and **(d)** vertical export flux of particulate organic carbon at 100 m (mol C m$^{-2}$ yr$^{-1}$); **(e)** and **(f)** exchange flux of $CO_2$ across the air-sea interface (mol C m$^{-2}$ yr$^{-1}$). Positive fluxes indicate outgassing.

The vertical extent of the phytoplankton bloom and its associated decreases in nitrate and DIC remains limited to the mixed layer, which is between only about 15 to 40 m deep in the fertilized region. Below the mixed layer, nitrate and DIC increase relative to the unperturbed case (Fig. 4), due to the remineralization of the extra organic matter that is sinking through the water column. Despite a substantial amount of shallow remineralization, roughly 10% of the fertilization induced enhancement of NPP within the fertilized patch is exported as particulate organic carbon to depths below 100 m (Fig. 3c, d).

The horizontal spreading of the fertilization induced perturbations in tracer distributions is even more extensive at depth than at the surface (Fig. 4). At 50 m depth, the changes in DIC and nitrate are characterized by concentration increases extending from the fertilization patch far toward the east, and by a region of decreased concentration southwest of the patch. The former is caused by the horizontal advection of the nitrate and DIC that has accumulated underneath the fertilized region, while the latter is caused by the reduction in productivity that occurred downstream (for surface flow) of the fertilized site (Fig. 3b) due to the depletion in surface nitrate (Fig. 2c, d).

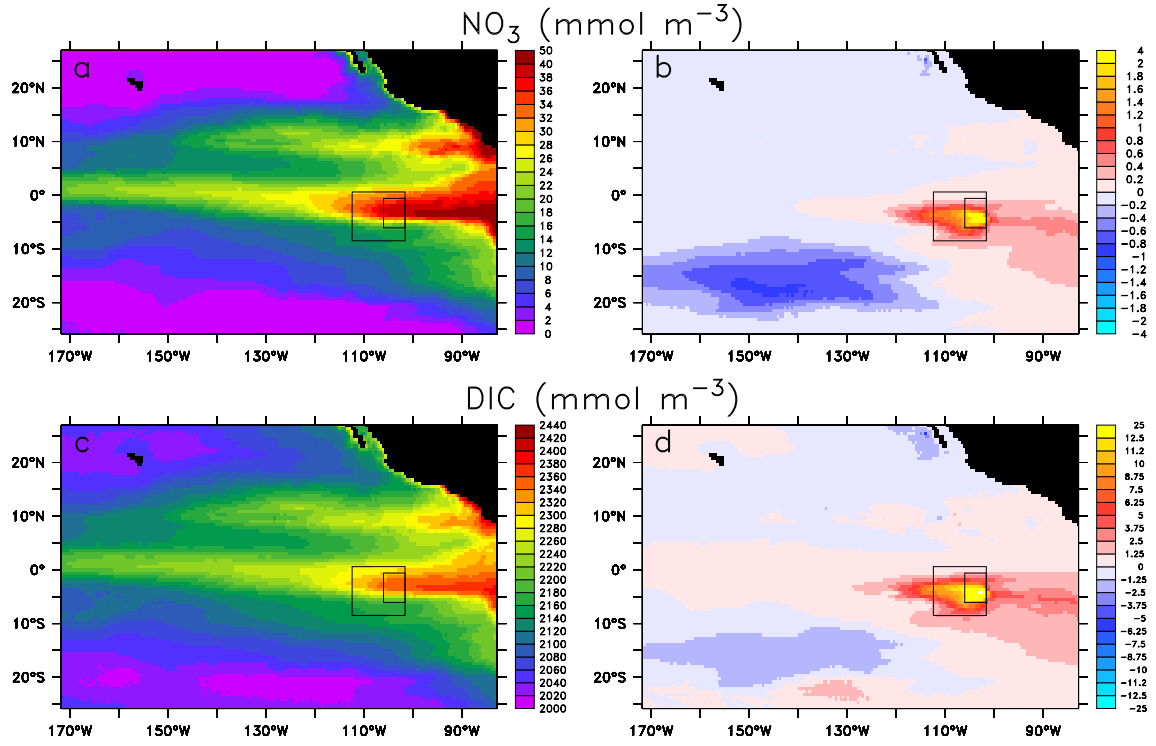


**Fig. 4.** As Fig. 2, except for properties at 50 m depth. **(a)** and **(b)** nitrate (mmol $m^{-3}$); **(c)** and **(d)** dissolved inorganic carbon (mmol $m^{-3}$).

### 4.2 Temporal changes

The areally integrated anomalous fluxes for the standard case (Fig. 5a) show a very rapid initial rise in response to the start of the iron fertilization, reaching a maximum near year 2. Thereafter, the fluxes remain essentially flat or decline gradually. The anomalous export fluxes of $CaCO_3$ and dissolved organic carbon (DOC) are much smaller than those for particulate organic carbon (POC), so that the POC export flux essentially determines the uptake efficiency. The changes in the POC and $CaCO_3$ fluxes are associated with relatively modest changes in the ecosystem structure. In particular, there is only a small change in the relative abundance of coccolithophorids, which would cause a change in the inorganic-to-organic carbon export ratio. Consequently, we therefore will not consider these ecosystem changes further.

Over 10 years, the continuous fertilization of the standard patch results in the removal of about 0.15 Pg C from the atmosphere (Table 2), which corresponds to a reduction in atmospheric $CO_2$ of only 0.07 ppm. This cumulative uptake is driven by an iron fertilization induced export of POC, DOC, and $CaCO_3$, which together amount to about 0.18 Pg C over 10 years. The ratio of these two cumulative fluxes is the atmospheric uptake efficiency, which turns out to be 0.81 for the standard case after 10 years. Figure 5c shows that for this case of continuous fertilization, the efficiency is relatively stable after 3–4 years, since both the air-sea $CO_2$ flux and the carbon export fluxes tend to decrease at similar rates. Therefore, we do not expect that longer integrations of the model will substantially alter the conclusions found here. We tested this assumption by continuing the iron fertilization in the STANDARD model for another 33 years for a total of 43 years. Over the course of these 33 years, the atmospheric uptake efficiency decreased only from 0.81 to 0.72, consistent with our expectation.

The time evolution of the carbon fluxes for the one-time fertilization (3MON-onetime) is fundamentally different (Fig. 5d). Although enhanced export of POC persists for nearly three years beyond the end of the addition of iron to the system, the subsequent years (4 through 10) are characterized by smaller than normal export production. The persistence of the enhanced export is due to the fact that a substantial fraction of the added iron remains in the upper ocean and is only slowly removed. However, after a few years, the slowly diminishing enhanced iron concentrations as well as the now decreased near surface concentration of macronutrients (such as nitrate) lead to a substantial reduction of export production, which takes more than 10 years to recover. This process has been referred to as the rebound period by Gnanadesikan et al. (2003) and is commonly observed in iron fertilization model experiments to study the effects of a one-time fertilization (e.g., Aumont and Bopp, 2006 and Matsumoto, 2006). The anomalous uptake of $CO_2$ from the atmosphere stops faster than the enhanced export. Despite

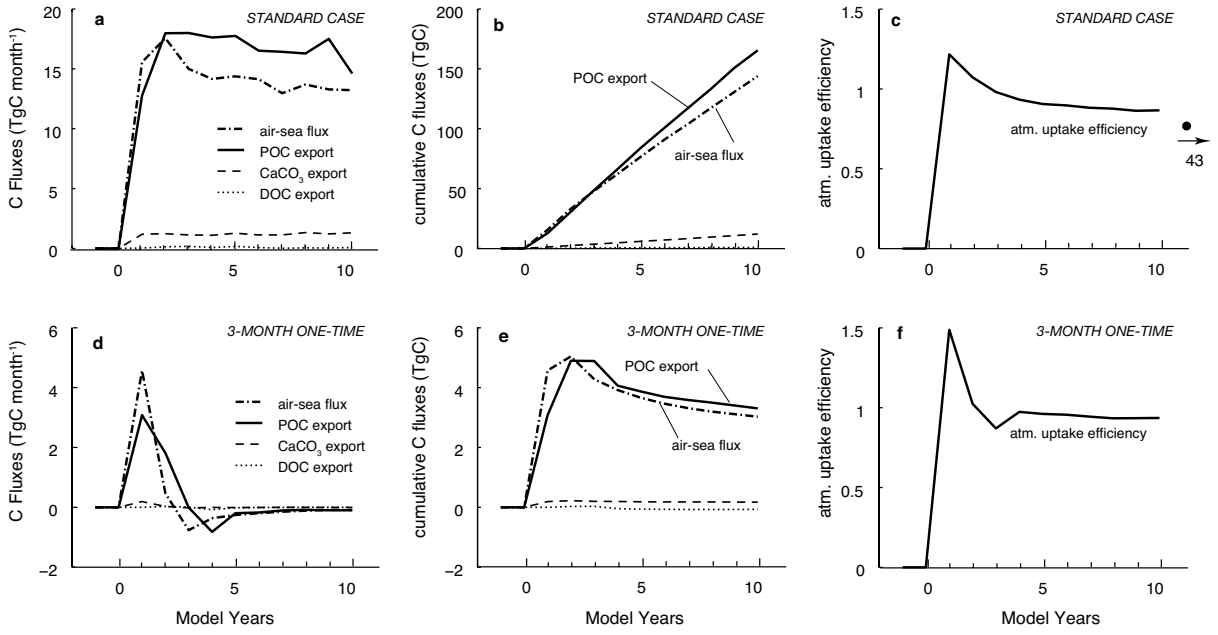


**Fig. 5.** Time series of carbon fluxes and efficiency for the STANDARD case (a–c), and for the 3MON-onetime case (d–f). **(a)** and **(d)** perturbation fluxes, **(b)** and **(e)** cumulative perturbation fluxes, **(c)** and **(f)** atmospheric uptake efficiency. Plotted are annual values.

POC export remaining elevated, the ocean starts to lose some of the gained $CO_2$ in year 3 and continues to do so for the rest of the 10 year simulation. These distinct temporal changes in the carbon fluxes result in a peak in the cumulative plots in year 2 and 3, respectively (Fig. 5e) and decreasing trends thereafter. Since the anomalous uptake of atmospheric $CO_2$ peaks faster and earlier than the anomalous downward export of carbon, the atmospheric uptake efficiency in this one-time fertilization has a distinct maximum in year 1 and decreases thereafter. However, since the cumulative fluxes of both air-sea exchange and vertical export decrease at a similar rate after year 3, the atmospheric uptake efficiency remains relatively constant thereafter.

The temporal evolution of the fluxes in the one-time case has implications for the different definitions of the atmospheric uptake efficiency. For example, Gnanadesikan et al. (2003) defined the atmospheric uptake efficiency as the ratio of the anomalous air-sea $CO_2$ flux integrated over the entire duration of the simulation and the anomalous POC export integrated over the duration of the iron fertilization only, i.e. they used different integration periods for the two fluxes. In our 3MON-onetime case, this definition would not take into account the substantial additional export of POC that occurs after the end of the fertilization, but it also would not take into account the decrease in POC export that occurs from year 3 onward. Over 10 years, Gnanadesikan's definition would yield an uptake efficiency of 1.60 for the 3MON-onetime case, which is much higher than what our definition of the atmospheric uptake efficiency yields (0.89) (see Table 2), representing the substantial net POC export that occurs after the end of the fertilization. In our 3MON-onetime case, the iron added into the ocean is still in the surface and plays a role in the iron fertilization for some time. A better estimate of anomalous POC export corresponding to Gnanadesikan's definition is to integrate it before it becomes negative (about 3 years). This produces an efficiency of 0.60. Since we fertilize (nearly) continuously for 10 years in all other cases, the different definitions have little impact on the results (Table 2).

### 4.3 Atmospheric uptake efficiencies

We compute the atmospheric uptake efficiency from the ratio of the areally and temporally integrated fluxes, thus,

$$e_{\text{uptake}} = \frac{\int_a \int_t \Delta\Phi^{\text{CO}_2}_{\text{air-sea}}\, da\, dt}{\int_a \int_t \Delta\Phi^{\text{C}_{\text{org}}+\text{CaCO}_3}_{\text{export}}\, da\, dt}, \quad (1)$$

where $\Delta\Phi^{\text{CO}_2}_{\text{air-sea}}$ is the change in the air-sea $CO_2$ flux in the fertilized case in comparison to the unfertilized case, and $\Delta\Phi^{\text{C}_{\text{org}}+\text{CaCO}_3}_{\text{export}}$ is the change in the export of biogenic carbon from the euphotic zone (assumed to be 100 m deep), consisting of the export of organic carbon in both particulate (POC) and dissolved forms (DOC), and mineral $CaCO_3$. The perturbation fluxes are integrated in time from the beginning of the fertilization until time $t$ and over the surface area $a$, in our case chosen as the entire domain of our Pacific model. The atmospheric uptake efficiency for our standard experiment amounts to 0.81, with the sensitivity experiments revealing that this efficiency can vary substantially in

**Table 2.** Summary of results: Listed are the anomalous fluxes as well as the computed efficiencies. Fluxes were integrated over 10 years and over the entire model domain and are given as differences from a control simulation.

| | STANDARD | TINY | SMALL | LARGE | X-LARGE | 3MON | | LIGHT-PERT | | | | PAC | |
|---|---|---|---|---|---|---|---|---|---|---|---|---|---|
| | | | | | (PAC) | repeat | onetime | LIGHT-UNLIM | | LIGHT-DEPTH | | 2×Fe | Iron-unlim |
| | | | | | | | | 75m | 50m | 2 | 4 | | |
| Fluxes (TgC for Carbon and Mmol for Fe) | | | | | | | | | | | | | |
| $\Delta\Phi^{CO_2}_{\text{air-sea}}$(TgC) | 143.9 | 1.3 | 44.5 | 1340.6 | 3443.4 | 39.2 | 3.0 | 96.8 | 69.8 | 11.7 | 44.1 | 1111.5 | 4569.0 |
| $\Delta\Phi^{\text{Fe}}_{\text{fert}}$ (Mmol) | 72.7 | 0.7 | 18.2 | 2246.2 | 31937.9 | 18.2 | 1.8 | 72.7 | 72.7 | 0.0 | 0.0 | 8003.6 | – |
| $\Delta\Phi^{\text{POC}}_{\text{export}}$(TgC) | 165.4 | 1.7 | 43.1 | 3218.4 | 10141.9 | 42.6 | 3.3 | 1627.1 | 271.4 | 308.8 | 850.5 | 2439.8 | 19184.4 |
| $\Delta\Phi^{\text{Ca}}_{\text{export}}$(TgC) | 12.0 | 0.1 | 5.2 | 133.1 | 414.8 | 1.9 | 0.2 | 185.9 | 137.5 | 1.5 | 4.0 | 20.9 | 308.4 |
| $\Delta\Phi^{\text{DOC}}_{\text{export}}$(TgC) | 0.8 | 0.0 | −0.2 | 83.0 | 398.1 | 0.1 | −0.1 | 495.9 | 106.0 | 23.1 | 48.9 | 126.9 | 740.5 |
| Efficiency | | | | | | | | | | | | | |
| $e_{\text{uptake}}$ | 0.81 | 0.75 | 0.93 | 0.39 | 0.31 | 0.88 | 0.89 | 0.04 | 0.14 | 0.04 | 0.05 | 0.43 | 0.23 |
| $e^{\text{regional}}_{\text{uptake}}$ [a] | 1.08 | 0.96 | 1.18 | – | – | 1.23 | 1.18 | 0.04 | 0.14 | −0.01 | −0.00 | – | – |
| $e^{\text{patch}}_{\text{uptake}}$ [b] | 0.77 | 0.32 | 0.50 | 0.47 | 0.31 | 0.87 | 0.81 | 0.04 | 0.10 | −0.00 | −0.00 | 0.43 | 0.23 |
| $\text{EFF}_{\text{depl}}$ [c] | 0.87 | 0.80 | 1.03 | 0.42 | 0.34 | 0.92 | 1.60[d] | 0.06 | 0.26 | 0.46 | 0.24 | | |
| Normalized Ratios [e] | | | | | | | | | | | | | |
| $r^{\text{C:Fe}}_{\text{util}}$ | 0.70 | 0.70 | 0.76 | 0.44 | 0.10 | 0.70 | 0.54 | – | – | – | – | 0.09 | – |
| $r^{\text{C:Fe}}_{\text{fert}}$ | 0.57 | 0.53 | 0.70 | 0.17 | 0.03 | 0.62 | 0.48 | – | – | – | – | 0.04 | – |

[a] Atmospheric uptake efficiency computed over the eastern tropical Pacific analysis region bounded by 101.6° W to 112.4° W, and 8.5° S to 0.6° N. This region has an area of $7.6\times10^5$ km$^2$.

[b] Atmospheric uptake efficiency computed over only the size of the fertilized patch.

[c] Depletion efficiency as defined by Gnanadesikan et al. (2003), i.e. $\text{EFF}_{\text{depl}} = \int_a \int_t \Delta\Phi^{\text{CO}_2}_{\text{air-sea}}\, da\, dt \,/\, \int_a \int_{t_{\text{fert}}} \Delta\Phi^{\text{POC}}_{\text{export}}\, da\, dt$, where $t_{\text{fert}}$ is the duration of the fertilization.

[d] Integrating anomalous POC export over only the first two years, and accounting only for enhanced POC export, the efficiency would be 0.6.

[e] The ratios were normalized with our control ratio of $r^{C:Fe}_{\text{ctrl}} = 2.9 \times 10^5$ mol C (mol Fe)$^{-1}$.

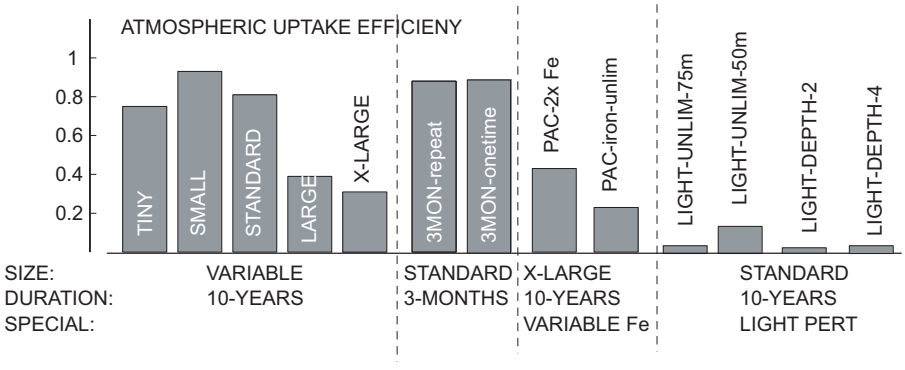


**Fig. 6.** Atmospheric uptake efficiencies of our simulations. Shown are the values after 10 years. Also listed are some of the key characteristics of the different simulations. Table 1 gives a complete description of each simulation.

response to changes in the size of the fertilized region, but that it changes only slightly in response to changes in the duration of the experiments (see Fig. 6, and Table 2). The difference between the most efficient (SMALL with an area of $92\times10^3$ km$^2$ and $e_{\text{uptake}}$=0.93) and the least efficient (X-LARGE with an area of $150\times10^6$ km$^2$ and $e_{\text{uptake}}$=0.31) is about a factor of 3. These differences will be explored in more detail in the discussion. By contrast, there is hardly a difference in the atmospheric uptake efficiency over ten years between the cases in which iron is added continuously (STANDARD: $e_{\text{uptake}}$=0.81), is added for 3 months every year (3MON-repeat: $e_{\text{uptake}}$=0.88), or is added only once for

3 months (3MON-onetime: $e_{\text{uptake}}$=0.89). Also the magnitude of the iron addition matters little. Doubling the magnitude of the iron added from the atmosphere results in only a small increase in the efficiency (0.43 in PAC-2×Fe versus 0.31 in X-LARGE), while the addition of iron until phytoplankton becomes iron unlimited leads to a moderate decrease (0.23 in PAC-iron-unlim).

Our range of atmospheric uptake efficiencies is similar to the values of 0.44 to 0.57 we infer from the recent global-scale iron flux sensitivity experiments of Moore et al. (2006). Thus, iron fertilization experiments that actually model the addition of iron explicitly are finding atmospheric uptake efficiencies that are consistently larger than those determined earlier, using a nutrient restoring approach (e.g., Gnanadesikan et al., 2003). As discussed above, the different definitions cannot explain the differences, because the contribution of the non-POC export fluxes are small, and because the different time integrations also have relatively little impact over ten years for experiments with continuous fertilization.

Another issue to consider is the area over which the fluxes are integrated. As shown in Table 2, the efficiencies are generally about 20% larger if the area used is only regional, i.e. is limited to the near-field of the patch. This is because the contribution of the anomalous outgassing far downstream of the patch is larger than the anomalous reduction of export production in the far-field. Limiting the areal integration to the actual fertilized patch yields efficiencies that are mostly smaller than either global or regional efficiencies. This is primarily a consequence of the region of anomalous uptake of $CO_2$ from the atmosphere being much larger than the patch itself, and also extending well beyond the region of enhanced export (cf. Fig. 3). Qualitatively, the sensitivity of the atmospheric uptake efficiency to changing integration area is similar in our simulations to that found by Gnanadesikan et al. (2003), but tend to be smaller. For example, Gnanadesikan et al. (2003) reported a factor of three difference in the efficiency depending on whether the efficiency was determined regionally or globally.

Given these differences and the substantial variations identified in our simulations, it behooves us to understand the processes that determine the uptake efficiency.

## 5 Discussion

As listed in the introduction, several factors control the magnitude of the atmospheric uptake efficiency: (i) The extent to which lateral and vertical transport of DIC, rather than uptake of $CO_2$ from the atmosphere, replaces the inorganic carbon that has been taken up by the fertilized phytoplankton, is converted to organic carbon and subsequently exported to depth. By definition, the higher the fraction of carbon that comes from the atmosphere, the larger is the atmospheric uptake efficiency. (ii) The extent to which the production and export of $CaCO_3$ is stimulated. Since the formation of $CaCO_3$ liberates an aqueous $CO_2$ molecule, this process will cause outgassing to the atmosphere (Zeebe and Archer, 2005; Millero, 2007; Sarmiento and Gruber, 2006). Therefore, any iron fertilization induced stimulation of $CaCO_3$ production and export would tend to reduce the atmospheric uptake efficiency. (iii) The extent of the changes in $pCO_2$ due to the carbonate system buffering. (iv) The extent to which the outgassing $CO_2$ from the surface ocean in response to the lowered atmospheric $CO_2$ reduces the net gain of $CO_2$ from the atmosphere. Additional factors that need to be considered are the timescale under consideration, and the duration of the fertilization.

The compensatory outgassing (iv) can be ruled out immediately as an explanation for the large differences in the atmospheric uptake efficiencies between the different sensitivity cases considered here, since our simulations were undertaken with a fixed atmospheric $pCO_2$. However, the compensatory efflux can explain part of the difference between our high uptake efficiencies and the low ones reported by e.g. Gnanadesikan et al. (2003). However, Sarmiento et al. (2008)[1] show that the consideration of a variable atmospheric $CO_2$ results only in a 20% reduction of the atmospheric uptake efficiency over 10 years, i.e. in our standard case, the efficiency would drop from 0.81 to 0.65. Though important, this cannot close the gap between our high efficiencies and the lower ones found in the previous nutrient-restoring based studies. The buffering effect of the ocean's carbonate system (iii) is also not responsible for the differences, since the carbonate chemistry between the different models and sensitivity cases is essentially the same. The $CaCO_3$ mechanism (ii) can be ruled out as well, since the stimulation of $CaCO_3$ production and export is relatively modest in our simulations (Fig. 5), and does not change much between the different cases considered. It also cannot explain the difference to Gnanadesikan et al. (2003) since their definition, which is based on the vertical export of POC alone, actually leads to higher efficiencies (see row $EFF_{\text{depl}}$ in Table 2). This essentially leaves the first mechanism, i.e. lateral/vertical supply versus atmospheric uptake of $CO_2$ as the primary explanation for the differences.

The lateral/vertical supply mechanism hypothesis creates some puzzles, however, as one initially would expect the atmospheric uptake efficiency to increase as the size of the fertilized region gets larger, exactly the opposite from what we found in our simulations. This expectation is based on the argument that the likelihood of an inorganic carbon atom to be supplied laterally into the fertilized region to replace an atom that has been taken up by phytoplankton and exported to depth will decrease as the fertilized region gets larger, because the lateral area that encloses the fertilized region decreases rapidly relative to its volume. In contrast, the ratio of the area of the air-sea interface relative to the volume of the fertilized region stays roughly the same, so that the likelihood of a $CO_2$ molecule to come from the atmosphere is roughly independent of the area of the fertilized region. Putting these

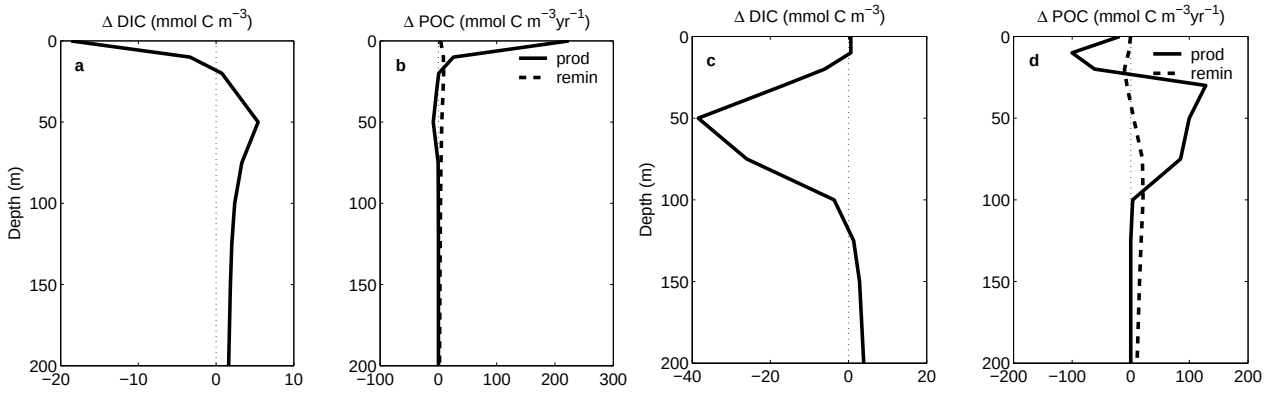


**Fig. 7.** Vertical profiles of anomalous properties averaged over the eastern tropical Pacific analysis region (101.6° W to 112.4° W and 8.5° S to 0.6° N) for the STANDARD case **(a)** and **(b)**, and for the LIGHT-DEPTH-2 case **(c)** and **(d)**. **(a)** and **(c)** Profiles of anomalous DIC, **(b)** and **(d)** Profiles of anomalous POC source-minus-sink terms (production and remineralization). In the LIGHT-DEPTH-2 case, the light dependent term of phytoplankton growth was manipulated in such a way that phytoplankton can get more light down to 75 m, resulting in a deep phytoplankton bloom. Shown are the results for our 10 year fertilization. Note the different scales for the two cases.

two trends together, one would expect the atmospheric uptake efficiency to increase with increasing size of the fertilized region.

The answer to the puzzle and to the discrepancies with previous low efficiencies lies in the vertical distribution of the changes, as the above argument is implicitly based on the assumption that the DIC changes induced by the fertilization extend from the surface down to the bottom of the euphotic zone, i.e. down to 100 m. However, as noted above, in our model iron fertilization induces a very shallow bloom, so that nutrients and inorganic carbon are removed only in the near-surface layers (Fig. 2). Most of this carbon is not moved to great depths, but actually accumulates right underneath the surface layer, still well within the euphotic zone (Fig. 4). This is illustrated in more detail in Fig. 7a, which shows that, when averaged over our eastern tropical Pacific analysis region (101.6° W to 112.4° W and 8.5° S to 0.6° N with an area of $7.6\times10^5$ km$^2$), DIC is depleted down to only 15 m, and that below this depth, DIC is actually elevated with a maximum just below 50 m. Analysis of the POC term balance in this region demonstrates that the rapid decrease of the net community production of POC (production minus respiration) with depth is the main cause of this strong vertical separation within the euphotic zone (Fig. 7b). Production of POC is enhanced just for the upper 20 m, while below this depth, the anomalous POC production is negative in the fertilized case relative to the control run. In contrast, the remineralization of POC is enhanced throughout all depths. This leads to the net balance of POC being positive (positive net community production) for only the top 15 m, while the net balance is negative (negative net community production) from 15 m downward to more than 200 m.

With most of the DIC drawdown occurring near the surface rather than near the bottom of the euphotic zone, the likelihood of the removed inorganic carbon atom to be replaced from the atmosphere is very high. Furthermore, only a fraction of the net production of organic matter that caused the near surface drawdown of DIC is actually exported below 100 m, elevating the atmospheric uptake efficiency as well. Therefore the high efficiencies in the tropical Pacific region are partly related to the shallow mixed layer depth there. The situations in other HNLC systems (N. Pacific, Southern Ocean), where the winter mixed layer depth matches or exceeds the euphotic depth, might be different. In fact, the low efficiency of the "whole Pacific" experiments, X-LARGE, might include this impact. In addition, the X-LARGE experiment includes a small stimulation of nitrogen fixation, albeit of small magnitude.

In order to assess our depth distribution hypothesis in more detail, we constructed a carbon budget for our eastern tropical Pacific analysis region, separating the upper ocean into a near-surface part (0–20 m) and a deeper part (20–100 m) of the euphotic zone (Fig. 8a). In our standard case, the iron fertilization stimulates an increase of net community production by 31.1 TgC yr$^{-1}$, and of $CaCO_3$ production by 1.1 TgC yr$^{-1}$. The corresponding DIC drawdown is compensated by uptake from the atmosphere (12.8 TgC yr$^{-1}$, 40%), horizontal transport (11.9 TgC yr$^{-1}$, 37%), and vertical mixing and transport from below (7.8 TgC yr$^{-1}$, 23%), respectively. Three quarters of the anomalous net community production is exported vertically below 20 m, with the remaining 25% being exported horizontally. Of the 24.6 TgC yr$^{-1}$ of carbon arriving from above in the lower part of the euphotic zone from 20 m to 100 m, the majority (55%) is remineralized, leaving only 12.8 TgC yr$^{-1}$ for export below 100 m (11.7 TgC yr$^{-1}$ as POC, 1.1 TgC yr$^{-1}$ as $CaCO_3$). Thus of the carbon exported from the top 20 m, only 48% comes from the atmosphere, while of the carbon exported from the entire

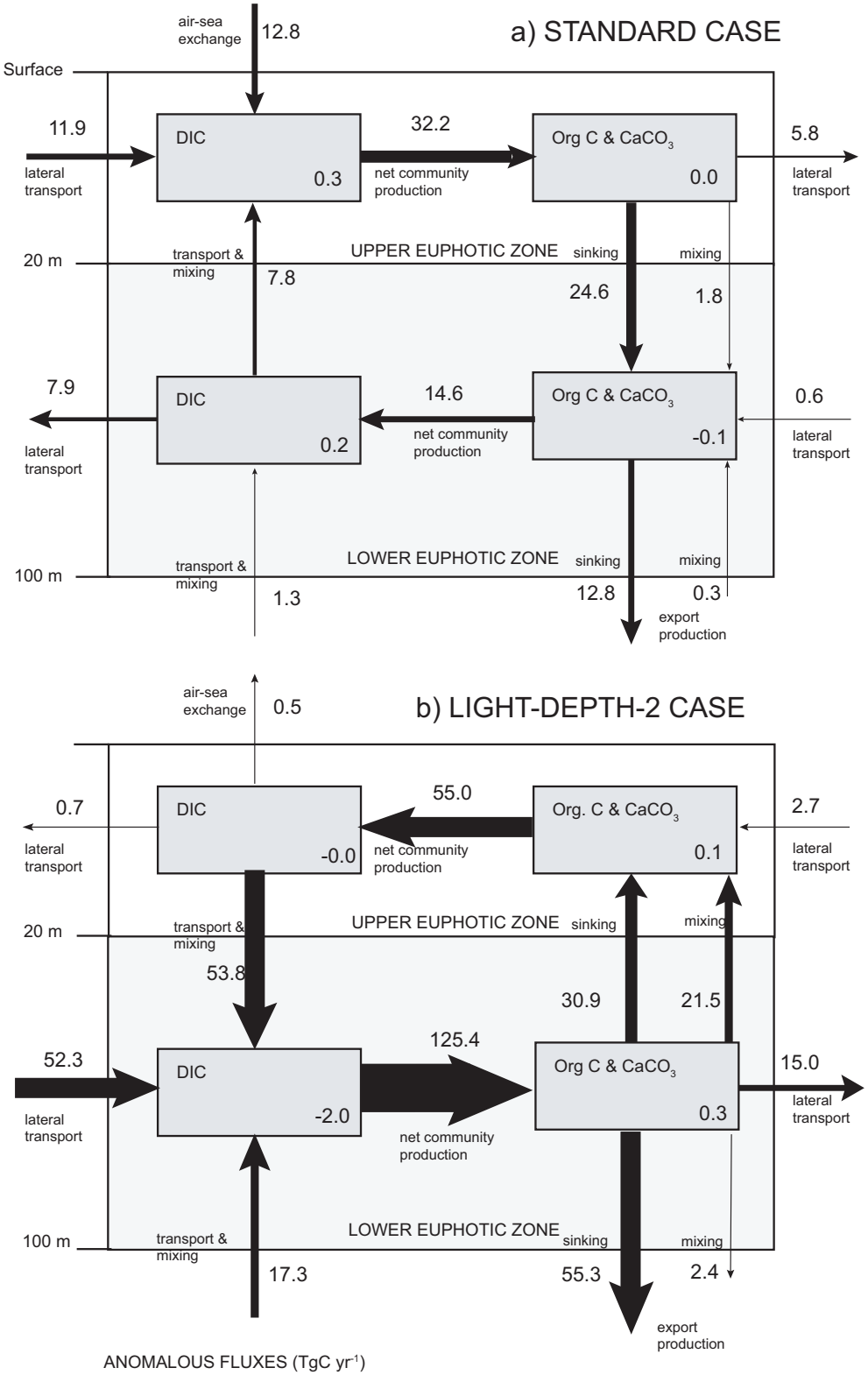


**Fig. 8.** Anomalous carbon budgets for the eastern tropical Pacific analysis region for the STANDARD case **(a)**, and for the LIGHT-DEPTH-2 case **(b)**. Separate budgets were computed for the upper part of the euphotic zone (above 20 m) and for the lower part of the euphotic zone (20 m to 100 m). The organic carbon and $CaCO_3$ fluxes are shown together, but the $CaCO_3$ flux usually makes up less than a few percent of the total flux. Shown are the fluxes for the 10th year after the start of the fertilization. The units for the anomalous fluxes are TgC $yr^{-1}$. At this time, the system is almost in steady state, the small derivative terms are shown in the lower right of each state variable box. The analysis region is bounded by 101.6° W and 112.4° W, and 8.5° S and 0.6° N extending over an area of $7.6 \times 10^5$ $km^2$.

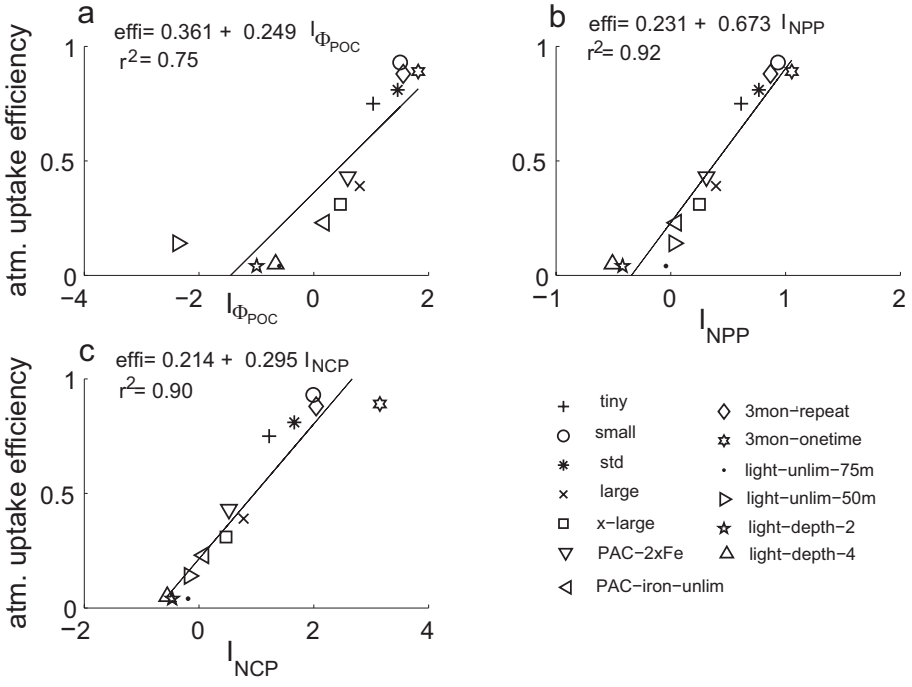


**Fig. 9.** Correlation of the atmospheric uptake efficiencies for all simulations with various indices of the vertical distribution of the fertilization induced changes in the biological pump (see Eq. (2) in the main text). These indices reflect what fraction of the changes over the entire euphotic layer occur in the top 10 m of the euphotic layer. Therefore, a uniform distribution would produce a value of 0.1. **(a)** Index based on the export flux of POC contributed from the layer (the differences between the bottom and top of the layer), $I_{\Phi_{POC}}$, **(b)** index based on net primary production, $I_{NPP}$, and **(c)** index based on net community production. Regression equations based on a least squares fit to the model results and their $r^2$ are shown in each panel.

euphotic zone, more than 100% comes from the atmosphere (see regional efficiency, $e^{regional}_{uptake}$ in Table 2).

This budget analysis supports our interpretation of why we get relatively high atmospheric uptake efficiencies: First, all of the export is stimulated in the near-surface layer, where the chance for a carbon atom to come from the atmosphere is much higher. Second, a high fraction of the carbon that is exported from the near surface layer remineralizes above 100 m, so that only a limited fraction continues to be exported across the 100 m horizon. It appears that this consequence of shallow remineralization on the magnitude of the export flux across the 100 m horizon is more important with respect to the atmospheric $CO_2$ uptake efficiency than the enhanced tendency of shallowly sequestered carbon to escape back to the atmosphere. An important reason for the apparently small loss rates of this shallowly sequestered carbon is the relatively good retention of the added iron. If iron is retained, it will continue to stimulate productivity whenever the waters containing the elevated DIC and iron surface, preventing the elevated DIC to escape to the atmosphere (see Appendix D for a more detailed discussion of iron retention).

Our depth distribution hypothesis not only explains the high atmospheric uptake efficiency of our STANDARD case, but also predicts successfully the variations in efficiency among our sensitivity cases (Fig. 9). More than 90% of the variance in the atmospheric uptake efficiency can be explained linearly by various indices, $I_P$, that express how much of the fertilization induced changes across the entire euphotic zone occur in the near-surface layer. These indices are defined as

$$I_P = \frac{\int_a \int_{z=0}^{z_{ul}} \Delta P \, da \, dz}{\int_a \int_{z=0}^{z_{euph}} \Delta P \, da \, dz} \quad (2)$$

where $z_{ul}$ is the depth of the upper part of the euphotic zone (here taken as 10 m), and $z_{euph}$ is the depth of the euphotic zone (here taken uniformly as 100 m). The indices are integrated over the area, $a$, that we used to calculate the atmospheric uptake efficiency, i.e. the entire domain of our Pacific model. The expression $\Delta P$ is the change in a particular property between the fertilization simulation and the control run. For $P$, we considered the production of organic carbon (net primary production, NPP), net community production (NCP), and the export flux of POC contributed from the layer (the differences between the bottom and top of the layer), $\Phi_{POC}$. If the fertilization induced changes are distributed homogeneously across the euphotic zone, $I_P$ would have a value of 0.1. Values above this indicate a distribution skewed toward the surface, while values below this indicate a distribution skewed toward the lower part of the euphotic zone. All three measures, i.e. $I_{NPP}$, $I_{NCP}$, and $I_{\Phi_{POC}}$ yield

very similar $r^2$, but with different linear regression equations (Fig. 9).

The largely explained variance thus suggests that the reason for the large changes in atmospheric uptake efficiencies with the different fertilized regions is that an increasing fraction of the total changes occur deeper in the euphotic zone and are no longer nearly exclusively restricted to the very near surface layer. These differences in depth distribution are owing to a number of processes, including deeper mixed layers and altered interaction between iron, light, and macronutrient limitation (e.g. Fe fertilization in regions with near-surface macronutrient limitation will stimulate phytoplankton production further down in the water column).

In order to further explore and test our hypothesis about the depth distribution of the stimulated export production controlling the atmospheric uptake efficiency, we analyze the light manipulation experiments (see Table 1). In all cases, the relief from light limitation results in a bloom that extends deep into the euphotic zone, causing, in the case of the LIGHT-DEPTH-2, a DIC depletion down to more than 100 m (Fig. 7c). The depth changes of POC production and remineralization (Fig. 7d) show enhanced growth in the lower parts of the euphotic zone, while POC production is actually reduced above 25 m. This is primarily due to the consumption of the macronutrients in the lower part of the euphotic zone, preventing these nutrients reaching the upper part of the euphotic zone. This effect is only partially reflected in the anomalous DIC profile (Fig. 7c), since the reduced biological consumption of DIC in the upper part of the euphotic zone is nearly offset by the reduced upward transport of DIC.

The carbon budget of the LIGHT-DEPTH-2 case illustrates the entirely different carbon dynamics of this deep phytoplankton bloom (Fig. 8b). Net community production in the upper 20 m decreases quite substantially, causing a reduction in the organic and inorganic carbon exported from this layer (this is equivalent to an anomalous upward transport of biogenic carbon). In contrast, net community production is strongly stimulated in the lower part of the euphotic zone, so that all of the vertical export of $55.3\,\mathrm{TgC\,yr^{-1}}$ across 100 m comes from this zone. Another $15\,\mathrm{TgC\,yr^{-1}}$ is exported laterally. This exported carbon is primarily replaced by lateral transport and by reduced mixing losses to the upper part of the euphotic zone, with some additional supply from below. The net effect on the air-sea exchange within the tropical Pacific analysis region is actually an anomalous outgassing, leading to a negative regional uptake efficiency. Outside the analysis region, the net effect is an anomalous uptake of $CO_2$, but the magnitude of this uptake flux is small, so that the global atmospheric uptake efficiency is only 0.04 (Table 2 and Fig. 6). Similarly low atmospheric uptake efficiencies are found for the other three light manipulation experiments with the exception of the LIGHT-UNLIM-50 m case, which has an atmospheric uptake efficiency of 0.14. However, this value is still smaller than that of any other simulation we have undertaken (Table 2 and Fig. 6). Although only approximately equivalent to the nutrient restoring approach used by most previous studies (Peng and Broecker, 1991; Joos et al., 1991; Sarmiento and Orr, 1991; Jin and Gruber, 2003; Gnanadesikan et al., 2003), these light manipulation simulations nevertheless suggest that perhaps the most important reason for the low atmospheric uptake efficiencies identified in these previous studies is the fact that their simulation setup tended to induce export stimulation in the deep parts of the euphotic zone. We tested this inference by conducting depth-dependent fertilization simulations with the nutrient restoring model of Jin and Gruber (2003) (the same model as that used by Gnanadesikan et al. (2003)). In a first set of cases, we restored the limiting macronutrient phosphate to zero over the entire euphotic zone as done in all previous studies. In a second set of cases, we restored phosphate to zero only in the surface layer of the model. For both sets, we conducted one-time (1 month) and continuous fertilizations for a duration of 10 years. The atmospheric uptake efficiencies over ten years from these sets of simulations clearly support our hypothesis, i.e. we find atmospheric uptake efficiencies in the near-surface fertilization cases that are three times larger than those from the entire euphotic zone fertilization cases, with little difference between the one time and continuous fertilizations. Budget analyses of these simulations show that these differences in the atmospheric uptake efficiencies are associated with the depth distribution of the anomalous production, with a more shallow distribution of the anomalous production favoring higher atmospheric uptake efficiencies.

Other factors, such as the "borrowing" of nutrients from other regions and other periods leading to reduced production downstream in time or space, a mechanism suggested by Gnanadesikan et al. (2003) and taken up by Aumont and Bopp (2006) can play only a minor role. If this mechanism were important, one would expect strong differences between one-time and continuous fertilizations, as the borrowing would follow different transport mechanisms (across time versus across space). No such differences are seen in our simulations, as there is little change between corresponding one-time and continuous fertilization simulations.

We thus conclude that the depth distribution of the changes in the biological pump is the key factor determining the atmospheric uptake efficiency with other factors contributing to it as well, but with lesser importance.

## 6 Summary and conclusions

The amount of $CO_2$ taken up from the atmosphere for a given change in the export of carbon by the ocean's biological pump, the atmospheric uptake efficiency, can vary greatly between less than 0.1 and more than 1. With the help of our experiments, we can explain a very large fraction of this variance in the atmospheric uptake efficiency by considering the depth distribution of the changes in the biological pump

within the euphotic zone. The higher up in the euphotic zone the biological pump is altered, the higher is the likelihood that an exported carbon atom comes from the atmosphere, i.e. the higher is the atmospheric uptake efficiency. Iron fertilization of near surface waters tends to induce very shallow blooms and export production, resulting in high atmospheric uptake efficiencies. The response is independent of the source of the additional near-surface iron input, which could come from the atmosphere, deliberate iron injection or shallow sediments.

While we believe that the identified mechanism to explain the differences in the atmospheric uptake efficiencies in our simulations is robust, we need to emphasize that the numerical values of the atmospheric uptake efficiencies need to be used with care. These values are applicable for only the ten year duration of our study, and they are upper-bound values due to our neglecting of an interactive atmosphere. With a variable atmosphere, the values need to be reduced by about 20% over ten years, and by about 50% over 100 years. In addition, the atmospheric uptake efficiency has a tendency to decrease on longer time-scales (>100 years). These effects need to be considered when applying our estimates to other situations.

A second finding we would like to comment on is that although the efficiency is high, the total amount of carbon that can be taken out of the atmosphere by iron fertilization is small. Even in the case of fertilization of the entire North and Tropical Pacific, the total air-sea flux over 10 years is only 3.4 Pg C. This supports the results of other iron fertilization experiments that also show small potential for changes in iron supply to alter atmospheric $CO_2$ (e.g., Aumont and Bopp, 2006; Bopp et al., 2003; Moore et al., 2006). When considering iron fertilization as a mitigation option, possible unintended ecological and biogeochemical consequences (Chisholm et al., 2001; Jin and Gruber, 2003; Schiermeier, 2003), legal constraints (Buesseler et al., 2008), as well as a full economic and societal cost/benefit analysis (Matsumoto, 2006) have to be considered as well.

Our findings have important implications for understanding and predicting the impact of changes in the biological pump on atmospheric $CO_2$. Although we have used primarily iron addition experiments as our tool to induce changes in the biological pump, the importance of the depth distribution in controlling the impact on atmospheric $CO_2$ of changes in the biological pump is largely independent of the actual mechanism that causes this change. Therefore, studies that investigate the impact of past or future changes in the biological pump on atmospheric $CO_2$ need to consider not only the changes in the export flux across the bottom of the euphotic zone, but also where within the euphotic zone the biological changes occur. A corollary to this is the need for modelers to pay more attention to the details of upper ocean physics and ecology/biogeochemistry in their models (Doney, 1999).

## Appendix A

### The efficiency of iron fertilization

A measure of the overall impact of the addition of iron on atmospheric $CO_2$ is the carbon-to-iron fertilization ratio, which describes how much additional $CO_2$ is taken up from the atmosphere for a given amount of iron added to the ocean (cf. Sarmiento et al. (2008)[1]):

$$R^{\mathrm{C:Fe}}_{\mathrm{fert}} = \frac{\int_a \int_t \Delta\Phi^{\mathrm{CO_2}}_{\mathrm{air\text{-}sea}}\, da\, dt}{\int_a \int_t \Delta\Phi^{\mathrm{Fe}}_{\mathrm{fert}}\, da\, dt}, \tag{A1}$$

where $\Delta\Phi^{\mathrm{CO_2}}_{\mathrm{air\text{-}sea}}$ is the change in the air-sea $CO_2$ flux in the fertilized case in comparison to the unfertilized case, and $\Delta\Phi^{\mathrm{Fe}}_{\mathrm{fert}}$ is the iron flux added to the ocean. The perturbation fluxes are integrated in time from the beginning of the fertilization until time $t$ and over the surface area $a$, usually chosen as the global surface ocean or in the case of regional models the entire model domain. Assuming that this fertilization ratio can be estimated well for any size and duration of an experiment, knowledge of its value would then permit to predict the net air-sea $CO_2$ flux that would result from any fertilization experiment, irrespective of whether it is of natural or human origin.

Since the process driving the perturbation in the air-sea $CO_2$ flux is the iron induced change in the biological export of carbon from the near surface ocean (euphotic zone), it is instructive to split the fertilization ratio into an efficiency part that reflects how much $CO_2$ is taken up from the atmosphere per unit change in biological export (termed the atmospheric uptake efficiency, $e_{\mathrm{uptake}}$), and into a biological iron utilization ratio that reflects how a given amount of added iron stimulates the biological export of carbon (termed the iron utilization ratio, $R^{\mathrm{C:Fe}}_{\mathrm{iron\ util}}$), thus:

$$e_{\mathrm{uptake}} = \frac{\int_a \int_t \Delta\Phi^{\mathrm{CO_2}}_{\mathrm{air\text{-}sea}}\, da\, dt}{\int_a \int_t \Delta\Phi^{\mathrm{C_{org}+CaCO_3}}_{\mathrm{export}}\, da\, dt}, \tag{A2}$$

$$R^{\mathrm{C:Fe}}_{\mathrm{iron\ util}} = \frac{\int_a \int_t \Delta\Phi^{\mathrm{C_{org}+CaCO_3}}_{\mathrm{export}}\, da\, dt}{\int_a \int_t \Delta\Phi^{\mathrm{Fe}}_{\mathrm{fert}}\, da\, dt}, \tag{A3}$$

where $\Delta\Phi^{\mathrm{C_{org}+CaCO_3}}_{\mathrm{export}}$ is the change in the biologically mediated export of carbon from the euphotic zone (assumed to be 100 m deep), consisting of the export of organic carbon in both particulate (POC) and dissolved forms (DOC), and mineral $CaCO_3$. By definition, the product of the atmospheric uptake efficiency and the biological iron utilization ratio is the fertilization ratio:

$$R^{\mathrm{C:Fe}}_{\mathrm{fert}} = e_{\mathrm{uptake}} \cdot R^{\mathrm{C:Fe}}_{\mathrm{iron\ util}}. \tag{A4}$$

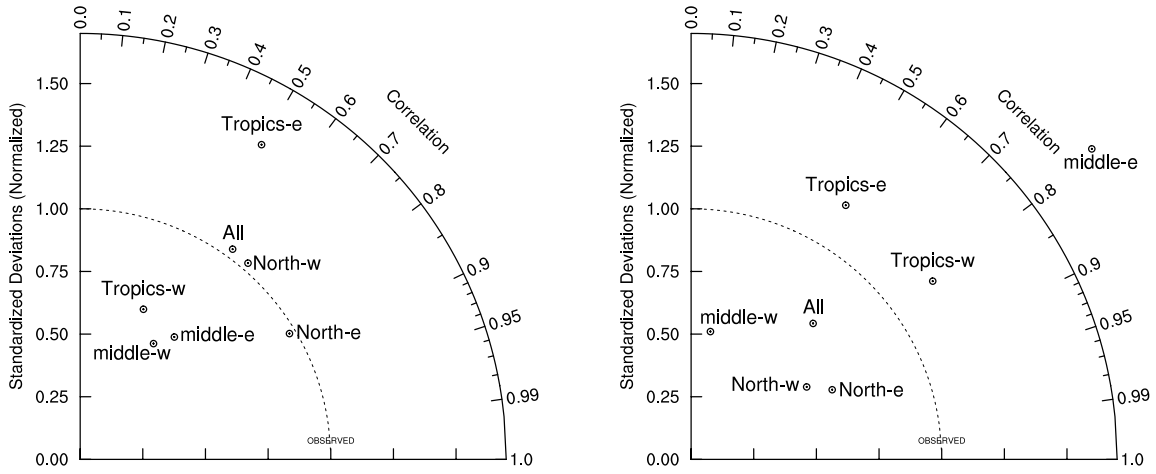


**Fig. 10.** Taylor diagrams of **(a)** chlorophyll and **(b)** nitrate, comparing annual mean modeled properties to annual mean observations from SeaWiFS in the case of chlorophyll, and an annual mean climatology from the World Ocean Atlas 2001 (WOA01) (Conkright et al., 2002) for nitrate. Shown are the comparisons for the entire model domain north of 10° S (All), as well as for a number of sub-domains: Tropics (10° S–10° N), middle (10° N–30° N), and North (30° N–65° N). Each of the three sub-domains are split into an eastern and a western sub-domain, with the boundary at 166° W. See text for an explanation of the Taylor diagram.

The atmospheric $CO_2$ uptake efficiency describes how the inorganic carbon that is lost to depth by the iron fertilization induced stimulation of biological export is replaced (see the discussion in the introduction section). The iron utilization ratio describes how iron added to the ocean stimulates the export of biogenic carbon. The value of this ratio depends on very complex processes, involving iron chemistry, especially the degree to which iron is scavenged from the water column relative to carbon and nutrients, phytoplankton metabolism, food web cycling, and the interaction of aphotic iron chemistry with large-scale ocean circulation and mixing (see Sarmiento et al. (2008)[1] for a more detailed discussion).

## Appendix B

### Taylor diagrams

A more quantitative assessment of the model's skill is provided by Taylor diagrams (Taylor, 2001) (Fig. 10a). These diagrams illustrate the level of agreement between the model and the observations in polar coordinates, with the correlation shown as the angle from the vertical in clockwise direction, and with the standard deviation of the modeled field relative to that of the observations shown as the distance from the origin. In such a diagram, the distance between the resulting end point and the point located on the abscissa at a relative standard deviation of 1 (representing a perfect match) is the root mean square (RMS) error of the model with regard to a particular set of observations. The correlation of annual mean chlorophyll between the model and the SeaWiFS derived observations for the entire Pacific north of 10° S is a respectable 0.60. The model's standard deviation of that pattern is nearly identical to that of the observations, giving a relative standard deviation of about 1. Splitting the model domain into sub-regions reveals that the level of agreement varies substantially within the Pacific. The lowest RMS error is found for the eastern North Pacific (>30° N, and east of 166° W), while the eastern tropical Pacific (10° S to 10° N, and east of 166° W) has the highest RMS error. The latter is largely due to the overestimation of chlorophyll by the model near the equator while the concentrations off the equator are similar, causing a much higher standard deviation in the model results compared to the observations.

The generally good agreement of model simulated and observed annual mean nitrate concentration is also illustrated more quantitatively by the Taylor diagram (Fig. 10b) (correlation of nearly 0.67, although with a standard deviation that is slightly lower than observed). As was the case for chlorophyll, analyses of the agreement between model results for nitrate and observations show large differences for the different regions, particularly with regard to the relative standard deviations.

## Appendix C

### Discussion of the model deficiencies

The deficiencies in the model are most likely due to the interaction of biases in the model physics with errors in the ecosystem/biogeochemical model. The overestimation of chlorophyll in the central equatorial Pacific is mostly caused by an overly strong equatorial upwelling in the model interacting with biology to create a nutrient trapping situation (Najjar et al., 1992), i.e. a situation in which nutrients that are

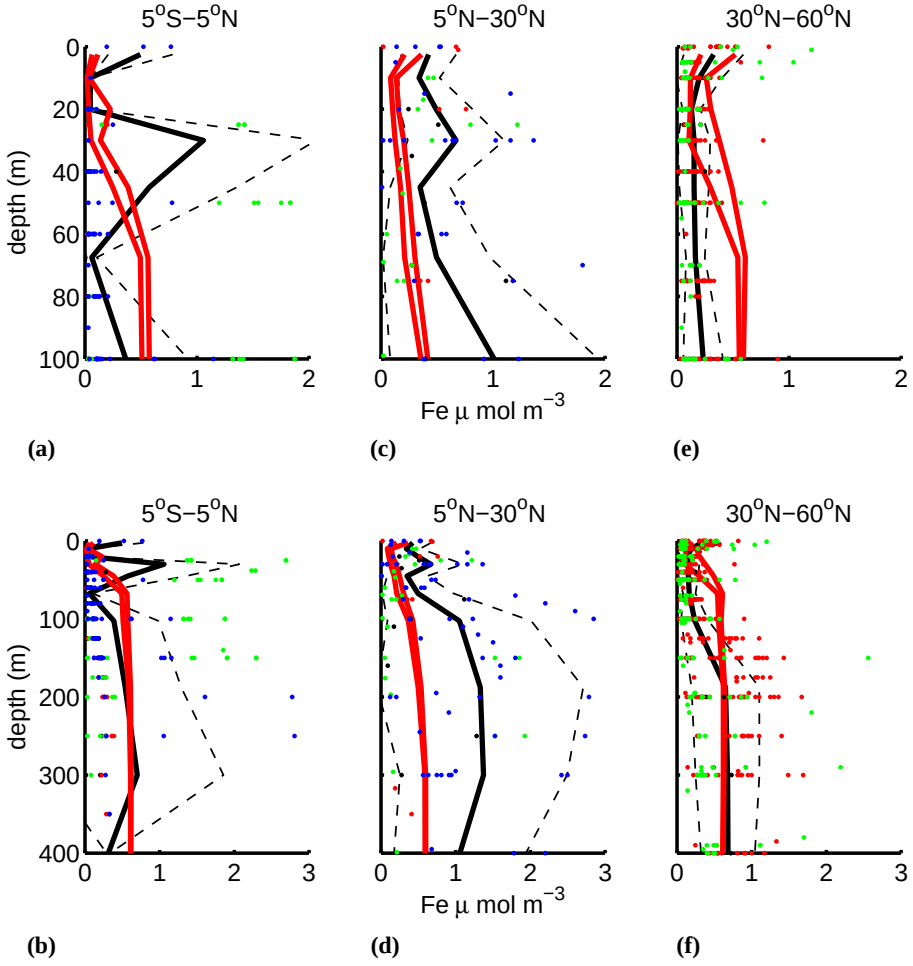


**Fig. 11.** Vertical profiles of dissolved iron, comparing model results with observations in three sub-domains of the Tropical and North Pacific. **(a)** and **(b)** 5° S to 5° N; **(c)** and **(d)** 5° to 30° N; and **(e)** and **(f)** 30° N to 60° N. The upper row shows the comparison for the upper 100 m only, whereas the bottom row depicts the data and model results for the upper 400 m. The area between two red lines indicates the range of model simulated dissolved iron at the locations where data are available. The black line is the mean of the observations with the dashed lines indicating the $\pm 1\sigma$ standard deviation. The dots are the actual observations with the color indicating the different seasons: black, winter (January–March); red, spring (April–June); green, summer (July–September); blue, fall (October–December). The data were taken from the summary provided by Parekh et al. (2004).

transported at depth toward the equator fail to escape from this region, leading to an enhancement of the sub-surface nitrate pool and consequently to increased productivity. The deficiencies in the subarctic Pacific are most likely due to the interaction between the physical model simulating insufficient upwelling inside the subpolar gyre of the North Pacific and the atmosphere providing too much bioavailable iron. As a result, the biological pump in the North Pacific is limited by iron to a lesser degree than thought (Boyd et al., 2004), permitting it to draw down the surface nutrients to levels below those observed. The main reason for the too far southward extent of the tongue of high nitrate is the lack of iron in the regions away from the equatorial axis of upwelling. Whatever iron is upwelled at the equator is rapidly consumed and exported downward again, leaving virtually no iron in the surface waters. As the upwelled waters contain an excess of nitrate relative to iron, not all nitrate is consumed, so that nitrate rich, but iron poor waters are advected poleward. Atmospheric deposition of iron in this region is extremely low, so that the HNLC conditions tend to persist until the poleward advected water masses are being mixed with subtropical waters containing elevated iron but lower nitrate concentrations (Fig. 2), providing for the necessary conditions to consume the remaining nitrate.

One possible explanation for the model simulating an overly broad HNLC region in the eastern tropical Pacific is that the concentration of iron in the waters that upwell near the equator is too low relative to nitrate, so that iron is depleted too quickly relative to nitrate. A second possibility is that the nitrogen-to-iron uptake ratios of the phytoplankton

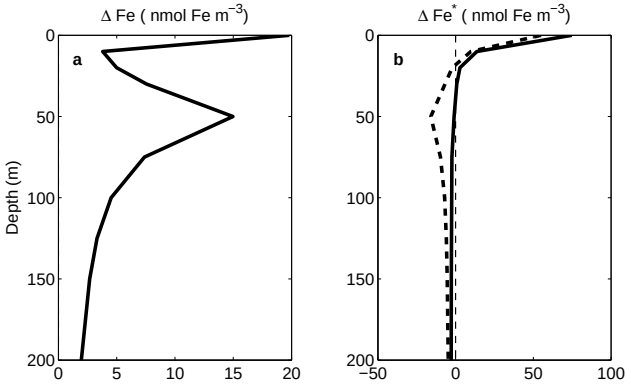


**Fig. 12.** Vertical profiles of anomalous iron parameters averaged over the eastern tropical Pacific analysis region for the STANDARD case. **(a)** Anomalous dissolved iron, and **(b)** $\Delta Fe^*$ (see text for definition) (solid line); $\Delta Fe^*$ if all iron was lost (dashed line). The quantity $\Delta Fe^*$ is a measure of the abundance of anomalous iron and anomalous dissolved inorganic carbon relative to the requirements for phytoplankton. Shown are the results for our 10 year fertilization.

growing near the equator is too low. A third possible explanation is that the atmospheric source of bio-available iron is underestimated, e.g. either because the dust deposition is too low, or because we have underestimated the fraction of iron that is bioavailable. Unfortunately, only few iron measurements exist in the ocean to differentiate among these different explanations. Those that exist (Fig. 11) suggest that the model may indeed underestimate the dissolved iron concentration in the upper ocean, particularly in the waters that upwell near the equator. This may be a consequence of the model having too low iron concentrations in the equatorial undercurrent, which has been described to transport substantial amounts of iron from the western into the eastern Pacific (e.g. Coale et al., 1996a). Since this iron likely originates from an exceptionally strong sedimentary source of the eastern Pacific Ocean (Mackey et al., 2002), which is not considered in our study, our model is bound to underestimate the iron concentration in the equatorial undercurrent. Additional factors, such as an underestimation of the bioavailable iron from dust may aggravate the iron limitation in the model, leading to the overly broad HNLC region in the tropical Pacific.

## Appendix D

### Iron retention

An important reason for the apparently small loss rates of this shallowly sequestered carbon is the relatively good retention of the added iron, as evidenced by the strong increase in the dissolved iron concentration in the region, where most of the sinking organic matter is remineralized (Fig. 12a). The degree to which iron is retained relative to carbon can be quantitatively assessed by the parameter $\Delta Fe^*$ (after Parekh et al., 2004), which describes how much anomalous iron is associated with the anomalous DIC relative to the requirements for phytoplankton, i.e. $\Delta Fe^* = \Delta Fe - r_{Fe:C} \times \Delta DIC$, where $r_{Fe:C}$ is the average iron-to-carbon uptake ratio of phytoplankton in our model ($3 \times 10^{-6}$ mol Fe (mol C)$^{-1}$). A $\Delta Fe^*$ of zero would thus mean that none of the iron got lost relative to carbon, while negative concentrations of $\Delta Fe^*$ are indicative of iron loss relative to carbon, creating a tendency for $CO_2$ loss to the atmosphere once this water gets back to the surface. The vertical profile of $\Delta Fe^*$ in Fig. 12b shows only moderately negative $\Delta Fe^*$ values in the subsurface (if all iron was lost, $\Delta Fe^*$ would have a maximum value of $-15$ nmol Fe m$^{-3}$ (computed as $-r_{Fe:C} \times \Delta DIC$ using the $\Delta DIC$ from the $\Delta DIC$ profile), so that only a small fraction of the sequestered carbon will escape to the atmosphere when these waters come back to the surface, while the remaining inorganic carbon is fixed again into organic carbon that can be exported back down to depth.

*Acknowledgements.* The majority of this work was funded by the Office of Science (BER) of the US Department of Energy through Grant No. DE-FG03-00ER63010. Additional funding was provided by the Information and Technology Research section of the US National Science Foundation (NG, HF, and SD) and ETH Zurich (NG). We are very grateful to Alexander (Sasha) F. Shchepetkin for his help with the Pacific setup of the Regional Oceanic Modeling System. We thank J. Sarmiento, F. Chavez, and M. Maltrud for stimulating discussions. Reviews by A. Gnanadesikan, O. Aumont and an anonymous reviewer helped to improve the paper and to sharpen our arguments. Computer time was made available by the National Center for Supercomputing Applications.

Edited by: J. Middelburg

## References

Armstrong, R. A., Lee, C., Hedges, J. I., Honjo, S., and Wakeham, S. G.: A new, mechanistic model for organic carbon fluxes in the ocean based on the quantitative association of POC with ballast minerals, Deep Sea Res. II, 49, 219–236, 2002.

Aumont, O. and Bopp, L.: Globalizing results from ocean in situ iron fertilization studies, Global Biogeochem. Cy., 20, GB2017, doi:10.1029/2005GB002591, 2006.

Aumont, O., Maier-Reimer, E., Blain, S., and Monfray, P.: An ecosystem model of the global ocean including Fe, Si, P co-limitations, Global Biogeochem. Cy., 17, 1060, doi:10.1029/2001GB001745, 2003.

Blain, S., Quéguiner, B., Armand, L., Belviso, S., Bombled, B., Bopp, L., Bowie, A., Brunet, C., Brussaard, C., Carlotti, F., Christaki, U., Corbiere, A., Durand, I., Ebersbach, F., Fuda, J.-L., Garcia, N., Gerringa, L., Griffiths, B., Guigue, C., Guillerm, C., Jacquet, S., Jeandel, C., Laan, P., Lefvère, D., Monaco, C. L., Malits, A., Mosseri, J., Obernosterer, I., Park, Y.-H., Picheral, M., Pondaven, P., Remenyi, T., Sandroni, V., Sarthou, G., Savoye, N., Scouarnec, L., Souhaut, M., Thuiller, D., Tim-

mermans, K., Trull, T., Uitz, J., van Beek, P., Veldhuis, M., Vincent, D., Viollier, E., Vong, L., and Wagener, T.: Effect of natural iron fertilization on carbon sequestration in the Southern Ocean, Nature, 446, 1070–1074, doi:10.1038/nature05700, 2007.

Bopp, L., Kohfeld, K. E., Le Quéré, C., and Aumont, O.: Dust impact on marine biota and atmospheric $CO_2$ during glacial periods, Paleoceanogr., 18, 1046, doi:10.1029/2002PA000810, 2003.

Boyd, P. W., Watson, A. J., Law, C. S., Abraham, E. R., Trull, T., Murdoch, R., Bakker, D. C. E., Bowie, A. R., Buesseler, K. O., Chang, H., Charette, M., Croot, P., Downing, K., Frew, R., Gall, M., Hadfield, M., Hall, J., Harvey, M., Jameson, G., Laroche, J., Liddicoat, M., Ling, R., Maldonado, M. T., McKay, R. M., Nodder, S., Pickmere, S., Pridmore, R., Rintoul, S., Safi, K., Sutton, P., Strzepek, R., Tanneberger, K., Turner, S., Waite, A., and Zeldis, J.: A mesoscale phytoplankton bloom in the polar Southern Ocean stimulated by iron fertilization, Nature, 407, 695–702, 2000.

Boyd, P. W., Law, C. S., Wong, C. S., Nojiri, Y., Tsuda, A., Levasseur, M., Takeda, S., Rivkin, R., Harrison, P., Strzepek, R., Gower, J., McKay, R. M., Abraham, E.,Arychuk, M., Barwell-Clarke, J., Crawford, W., Crawford, D., Hale, M., Harada, K., Johnson, K., Kiyosawa, H., Kudo, I., Marchetti, A., Miller, W., Needoba, J., Nishioka, J., Ogawa, H., Page, J., Robert, M., Saito, H., Sastri, A., Sherry, N., Soutar, T., Sutherland, N., Taira, Y., Whitney, F., Wong, C. S., and Yoshimura, T.: The decline and fate of an iron-induced subarctic phytoplankton bloom, Nature, 428, 549–553, 2004.

Boyd, P. W., Strzepek, R., Takeda, S., Jackson, G., Wong, C. S., McKay, R. M., Law, C., Kiyosawa, H., Saito, H., Sherry, N., Johnson, K., Gower, J., and Ramaiah, N.: The evolution and termination of an iron-induced mesoscale bloom in the northeast subarctic Pacific, Limnol. Oceanogr., 50, 1872–1886, 2005.

Boyd, P. W., Jickells, T., Law, C. S., Blain, S., Boyle, E. A., Buesseler, K. O., Coale, K. H., Cullen, J. J., de Baar, H. J. W., Follows, M., Harvey, M., Lancelot, C., Levasseur, M., Owens, N. P. J., Pollard, R., Rivkin, R. B., Sarmiento, J., Schoemann, V., Smetacek, V., Takeda, S., Tsuda, A., Turner, S., and Watson, A. J.: Mesoscale Iron Enrichment Experiments 1993-2005: Synthesis and Future Directions, Science, 315, 612–617, doi: 10.1126/science.1131669, 2007.

Buesseler, K. O. and Boyd, P. W.: Will Ocean Fertilization Work?, Science, 300, 67–68, 2003.

Buesseler, K. O., Doney, S. C., Karl, D. M., Boyd, P. W., Caldeira, K., Chai, F., Coale, K. H., de Baar, H. J. W., Falkowski, P. G., Johnson, K. S., Lampitt, R. S., Michaels, A. F., Naqvi, S. W. A., Smetacek, V., Takeda, S., and Watson, A. J.: Ocean Iron Fertilization-Moving forward in a sea of uncertainty, Science, 319, p. 162, 2008.

Chisholm, S. W., Falkowski, P. G., and Cullen, J. J.: Dis-Crediting Ocean Fertilization, Science, 294, 309–310, 2001.

Coale, K. H., Fitzwater, S. E., Gordon, R. M., Johnson, K. S., and Barber, R. T.: Control of community growth and export production by upwelled iron in the equatorial Pacific Ocean, Nature, 379, 621–624, 1996a.

Coale, K. H., Johnson, K. S., Fitzwater, S. E., Gordon, R. M., Tanner, S., Chavez, F. P., Ferioli, L., Sakamoto, C., Rogers, P., Millero, F., Steinberg, P., Nightingale, P., Cooper, D., Cochlan, W. P., Landry, M. R., Constantinou, J., Rollwagen, G., Trasvina, A., and Kudela, R.: A massive phytoplankton bloom induced by an ecosystem-scale iron fertilization experiment in the equatorial Pacific Ocean, Nature, 383, 495–501, 1996b.

Coale, K. H., Johnson, K. S., Chavez, F. P., Buesseler, K. O., Barber, R. T., Brzezinski, M. A., Cochlan, W. P., Millero, F. J., Falkowski, P. G., Bauer, J. E., Wanninkhof, R. H., Kudela, R. M., Altabet, M. A., Hales, B. E., Takahashi, T., Landry, M. R., Bidigare, R. B., Wang, X., Chase, Z., Strutton, P. G., Friederich, G. E., Gorbunov, M. Y., Lance, V. P., Hilting, A. K., Hiscock, M. R., Demarest, M., Hiscock, W. T., Sullivan, K. F., Tanner, S. J., Gordon, R. M., Hunter, C. N., Elrod, V. A., Fitzwater, S. E., Jones, J. L., Tozzi, S., Koblizek, M., Roberts, A. E., Herndon, J., Brewster, J., Ladizinsky, N., Smith, G., Cooper, D., Timothy, D., Brown, S. L., Selph, K. E., Sheridan, C. C., Twining, B. S., and Johnson, Z. I.: Southern Ocean Iron Enrichment Experiment: Carbon Cycling in High- and Low-Si Waters, Science, 304, 408–414, 2004.

Conkright, M. E., Locarnini, R. A., Garcia, H., O'Brien, T. O., Boyer, T., Stephens, C., and Antonov, J.: World Ocean Atlas 2001: Objective Analyses, Data Statistics, and Figures, CD-ROM Documentation, Tech. rep., National Oceanographic Data Center, Silver Spring, MD, 2002.

de Baar, H. J. W., Boyd, P. W., Coale, K. H., Landry, M. R., Tsuda, A., Assmy, P., Bakker, D. C. E., Bozec, Y., Barber, R. T., Brzezinski, M. A., Buesseler, K. O., Boye, M., Croot, P. L., Gervais, F., Gorbunov, M. Y., Harrison, P. J., Hiscock, W. T., Laan, P., Lancelot, C., Low, C. S., Levasseur, M., Marchetti, A., Millero, F. J., Nishioka, J., Nojiri, Y., van Oijen, T., Riebesell, U., Rijkenverg, M. J. A., Saito, H., Takeda, S., Timmermans, K. R., Veldhuis, M. J. W., Waite, A. M., and Wong, C. S.: Synthesis of iron fertilization experiments: From the iron age in the age of enlightenment, J. Geophys. Res., 110, C09S16, doi:10.1029/2004JC002601, 2005.

Doney, S. C.: Major challenges confronting marine biogeochemical modeling, Global Biogeochem. Cy., 13, 705–714, 1999.

Dutkiewicz, S., Follows, M. J., and Parekh, P.: Interactions of the iron and phosphorus cycles: A three-dimensional model study, Global Biogeochem. Cy., 19, GB1021, doi:10.1029/2004GB002342, 2005.

Gnanadesikan, A., Sarmiento, J. L., and Slater, R. D.: Effects of patchy ocean fertilization on atmospheric carbon dioxide and biological production, Global Biogeochem. Cy., 17, 1050, doi:10.1029/2002GB001940, 2003.

Gregg, W. W., Ginoux, P., Schopf, P. S., and Casey, N. W.: Phytoplankton and iron: validation of a global three-dimensional ocean biogeochemical model, Deep Sea Res. II, 50, 3143–3169, 2003.

Gruber, N. and Sarmiento, J. L.: Biogeochemical/Physical Interactions in Elemental Cycles, in: THE SEA: Biological-Physical Interactions in the Oceans, Vol. 12, edited by: Robinson, A. R., McCarthy, J. J., and Rothschild, B. J., John Wiley and Sons, New York, 337–399, 2002.

Haidvogel, D. B., Arango, H., Hedstrom, K., Beckmann, A., Malanotte-Rizzoli, P., and Shchepetkin, A. F.: Model evaluation experiments in the North Atlantic Basin: Simulations in nonlinear terrain-following coordinates, Dyn. Atmos. Oceans, 32, 239–281, 2000.

Jin, X. and Gruber, N.: Offsetting the radiative benefit of ocean iron fertilization by enhancing $N_2O$ emissions, Geophys. Res. Lett., 30, 2249, doi:10.1029/2003GL018458, 2003.

Joos, F., Sarmiento, J. L., and Siegenthaler, U.: Estimates of the

effect of Southern Ocean iron fertilization on atmospheric $CO_2$ concentrations, Nature, 349, 772–775, 1991.

Joos, F., Plattner, G.-K., Stocker, T. F., Marchal, O., and Schmittner, A.: Global warming and marine carbon cycle feedbacks on future atmospheric $CO_2$, Science, 284, 464–467, 1999.

Kalnay, E., Kanamitsu, M., Kistler, R., Collins, W., Deaven, D., Gandin, L., Iredell, M., Saha, S., White, G., Woollen, J., Zhu, Y., Chelliah, M., Ebisuzaki, W., Higgins, W., Janowiak, J., Mo, K. C., Ropelewski, C., Wang, J., Leetma, A., Reynolds, R., Jenne, R., and Joseph, D.: The NCEP/NCAR 40-year reanalysis project, B. Am. Meteorol. Soc., 77, 437–471, 1996.

Key, R. M., Kozyr, A., Sabine, C., Lee, K., Wanninkhof, R., Bullister, J., Feely, R., Millero, F., Mordy, C., and Peng, T.-H.: A global ocean carbon climatology: Results from Global Data Analysis Project (GLODAP), Global Biogeochem. Cy., 18, GB4031, doi:10.1029/2004GB002247, 2004.

Kohfeld, K. E., Le Quéré, C., Harrison, S. P., and Anderson, R. F.: Role of marine biology in glacial-interglacial $CO_2$ cycles, Science, 308, 74–78, 2005.

Luo, C., Mahowald, N. M., and del Corral, J.: Sensitivity study of meteorological parameters on mineral aerosol mobilization, transport, and distribution, J. Geophys. Res., 108, 4447, doi:10.1029/2003JD003483, 2003.

Mackey, D. J., O'Sullivan, J. E., and Watson, R. J.: Iron in the western Pacific: a riverine or hydrothermal source for iron in the Equatorial Undercurrent?, Deep Sea Res. I, 49, 877–893, 2002.

Martin, H. M., Gordon, R. M., and Fitzwater, S. E.: Iron in Antarctic waters, Nature, 345, 156–158, 1990.

Martin, J. H.: Glacial-interglacial $CO_2$ change: the iron hypothesis, Paleoceanogr., 5, 1–13, 1990.

Martin, J. H., Coale, K. H., Johnson, K. S., Fitzwater, S. E., Gordon, R. M., Tanner, S. J., Hunter, C. N., Elrod, V. A., Nowicki, J. L., Coley, T. L., Barber, R. T., Lindley, S., Watson, A. J., Scoy, K. V., Law, C. S., Liddicoat, M. I., Ling, R., Stanton, T., Stockel, J., Collins, C., Anderson, A., Bidigare, R., Ondrusek, M., Latasa, M., Millero, F. J., Lee, K., Yao, W., Zhang, J. Y., Friederich, G., Sakamoto, C., Chavez, F., Buck, K., Kolber, Z., Greene, R., Falkowski, P., Chisholm, S. W., Hoge, F., Swift, R., Yungel, J., Turner, S., Nightingale, P., Hatton, A., Liss, P., and Tindale, N. W.: Testing the iron hypothesis in ecosystems of the equatorial Pacific Ocean, Nature, 371, 123–129, 1994.

Matsumoto, K.: Model simulations of carbon sequestration in the northwest Pacific by patch fertilization, J. Oceanogr., 62, 887–902, 2006.

Millero, F. J.: The marine inorganic carbon cycle, Chem. Rev., 107, 308–341, 2007.

Moore, J. K., Doney, S. C., and Lindsay, K.: Upper ocean ecosystem dynamics and iron cycling in a global three-dimensional model, Global Biogeochem. Cy., 18, GB4028, doi:10.1029/2004GB002220, 2004.

Moore, J. K., Doney, S. C., Lindsay, K., Mahowald, N., and Michaels, A. F.: Nitrogen fixation amplifies the ocean biogeochemical response to decadal timescale variations in mineral dust deposition, Tellus B, 58, 560–572, doi:10.1111/j.1600-0889.2006.00209.x, 2006.

Murnane, R. J., Sarmiento, J. L., and Le Quéré, C.: Spatial distribution of air-sea fluxes and the interhemispheric transport of carbon by the oceans, Global Biogeochem. Cy., 13, 287–305, 1999.

Najjar, R. G., Sarmiento, J. L., and Toggweiler, J. R.: Downward transport and fate of organic matter in the ocean: Simulations with a general circulation model, Global Biogeochem. Cy., 6, 45–76, 1992.

Orr, J. and Sarmiento, J. L.: Potential of marine macroalgae as a sink for $CO_2$: constraints from a 3-D general circulation model of the global ocean, Water Air Soil Poll., 64, 405–421, 1992.

Parekh, P., Follows, M. J., and Boyle, E.: Modeling the global ocean iron cycle, Global Biogeochem. Cy., 18, GB1002, doi:10.1029/2003GB002061, 2004.

Peng, T.-H. and Broecker, W. S.: Factors limiting the reduction of atmospheric $CO_2$ by iron fertilization, Limnol. Oceanogr., 36, 1919–1927, 1991.

Plattner, G.-K., Joos, F., Stocker, T. F., and Marchal, O.: Feedback mechanisms and sensitivities of ocean carbon uptake under global warming, Tellus B, 53, 564–592, 2001.

Sarmiento, J. L. and Gruber, N.: Ocean Biogeochemical Dynamics, Princeton University Press, Princeton, New Jersey, 2006.

Sarmiento, J. L. and Orr, J. C.: Three-dimensional simulations of the impact of Southern Ocean nutrient depletion on atmospheric $CO_2$ and ocean chemistry, Limnol. Oceanogr., 36, 1928–1950, 1991.

Sarmiento, J. L. and Toggweiler, J. R.: A new model for the role of the oceans in determining atmospheric $pCO_2$, Nature, 308, 621–624, 1984.

Sarmiento, J. L., Hughes, T. M. C., Stouffer, R. J., and Manabe, S.: Simulated response of the ocean carbon cycle to anthropogenic climate warming, Nature, 393, 245–249, 1998.

Schiermeier, Q.: The oresmen, Nature, 421, 109–110, 2003.

Shchepetkin, A. F. and McWilliams, J. C.: The regional oceanic modeling system (ROMS): a split-explicit, free-surface, topography-following-coordinate oceanic model, Ocean Model., 9, 347–404, 2005.

Sigman, D. M. and Haug, G. H.: Biological pump in the past, in: Treatise On Geochemistry, edited by: Holland, H. D., Turekian, K. K., and Elderfield, H., Elsevier Sci., New York, 491–528, 2003.

Taylor, K. E.: Summarizing multiple aspects of model performance in a single diagram, J. Geophys. Res., 106, 7183–7192, 2001.

Zeebe, R. E. and Archer, D.: Feasibility of ocean fertilization and its impact on future atmospheric $CO_2$ levels, Geophys. Res. Lett., 32, L09703, doi:10.1029/2005GL022449, 2005.